Eugenol mimics exercise to promote skeletal muscle fiber remodeling and myokine IL-15 expression by activating TRPV1 channel

Tengteng Huang [§], Xiaoling Chen [§], Jun He, Ping Zheng, Yuheng Luo, Aimin Wu, Hui Yan, Bing Yu, Daiwen Chen, Zhiqing Huang [*]

Key Laboratory for Animal Disease-Resistance Nutrition of China Ministry of Education, Institute of Animal Nutrition, Sichuan Agricultural University, Chengdu, Sichuan 611130, P. R. China

[§] These authors contributed equally to this work.

[*]**Correspondence**: Zhiqing Huang, Institute of Animal Nutrition, Sichuan Agricultural University, Chengdu, Sichuan 611130, P. R. China; Tel/Fax: 86-28-86290922; E-mail: zqhuang@sicau.edu.cn

Abstract

Metabolic disorders are highly prevalent in modern society. Exercise mimetics are defined as pharmacologic compounds that can produce the beneficial effects of fitness. Recently, there has been increased interest in the role of eugenol and transient receptor potential vanilloid 1 (TRPV1) in improving metabolic health. The aim of this study was to investigate whether eugenol acts as an exercise mimetic by activating TRPV1. Here, we showed that eugenol improved endurance capacity, caused the conversion of fast to slow muscle fibers, and promoted white fat browning and lipolysis in mice. Mechanistically, eugenol promoted muscle fiber type transformation by activating TRPV1-mediated CaN signaling pathway. Subsequently, we identified IL-15 as a myokine that is regulated by the CaN/Nuclear factor of activated T cells cytoplasmic 1 (NFATc1) signaling pathway. Moreover, we found that TRPV1-mediated CaN/NFATc1 signaling, activated by eugenol, controlled IL-15 levels in C2C12 myotubes. Our results suggest that eugenol may act as an exercise mimetic to improve metabolic health via activating the TRPV1-mediated CaN signaling pathway.

Keywords: eugenol, exercise mimetic, IL-15, myokines, skeletal muscle fiber remodeling, TRPV1

Introduction

Due to the lack of regular exercise among many individuals (***Carlson et al., 2010***), metabolic diseases are highly prevalent in modern society (***Hoehn et al., 2010***). To address this issue, pharmacological interventions have been considered as potential treatments. Exercise mimetics are pharmacologic compounds that produce fitness benefits (***Fan and Evans, 2017***). Although some synthetic exercise mimetics such as AICAR (AMPK activator), GW501516 (PPARδ activator), SRT1720 (SIRT1 activator), and GSK4716 (ERRγ activator) have been used to improve fitness (***Feige et al., 2008; Narkar et al., 2008; Rangwala et al., 2010***), the safety and health of each drug must be considered. In recent years, plant extracts such as resveratrol, lycium barbarum and epicatechin have demonstrated potential as a new class of low-toxin exercise mimetics (***Meng et al., 2020; Nogueira et al., 2011; Wen et al., 2020***). Therefore, it is of great significance to discover natural medicinal and edible plants that have mimetic effects of exercise.

Based on their metabolism and contractile properties, muscle fibers are commonly divided into slow oxidative fibers (muscle fibers that express myosin heavy chain (MyHC) I) and fast glycolytic/oxidative fibers (muscle fibers that express MyHC IIa, MyHC IIx, or MyHC IIb) (***Schiaffino and Reggiani, 2011***). Different muscle fibers exhibit a high degree of plasticity and are regulated by exercise (***Egan and Zierath, 2013***). The increased proportion of slow muscle fibers contributes to the enhancement of mitochondrial biogenesis and lipid metabolism (***Carlson et al., 2010***). Therefore, one of the benefits of exercise is to treat metabolic disorders by promoting slow muscle fiber remodeling (***Duan et al., 2017***). In addition, it has been increasingly recognized that myokines released by skeletal muscle play an essential role in mediating the benefits of exercise. Myokines are defined as cytokines or peptides that are released from skeletal muscle cells, which exert autocrine, paracrine, or endocrine effects (***Pedersen and Febbraio, 2012***). As a medium of crosstalk between muscles and other organs, myokines exert systemic regulation of exercise by acting on the muscle, fat, liver, pancreas, and other organs, effectively

61 improving insulin resistance, obesity, and metabolic disorders of type 2 diabetes (***Severinsen and***
62 ***Pedersen, 2020***). Therefore, another potential effect of exercise is to induce the release of
63 myokines (***Fan and Evans, 2017***). Although many previous studies have discovered plant
64 extracts as exercise mimetics by promoting slow oxidative muscle fiber, few studies have
65 investigated the effect of exercise mimetics on the release of myokines.

66 Eugenol is a safe natural compound extracted from clove oil and various plant spices such as
67 basil, bay leaves, and cinnamon (***Kaur et al., 2010***). Eugenol exhibits a variety of biological
68 activities, including antioxidative (***Magalhães et al., 2019***), antibacterial (***Devi et al., 2010***), anti-
69 inflammatory (***Magalhães et al., 2019***) and anti-cancer activities (***Lesgards et al., 2014***). Recent
70 studies have also suggested that eugenol could be a promising therapeutic drug for preventing
71 diabetes and obesity (***Al-Trad et al., 2019; Jung et al., 2012; Mnafgui et al., 2013; Srinivasan et***
72 ***al., 2014***), indicating its potential as an exercise mimetic. In addition. as a member of the transient
73 receptor potential (TRP) channel family, TRP vanilloid 1 (TRPV1), also known as the capsaicin
74 receptor, has been reported to improve endurance capacity and energy metabolism (***Luo et al.,***
75 ***2012***), counter obesity (***Baskaran et al., 2016***), and intervene diabetes (***Wang et al., 2012***),
76 making it a potential target protein for discovering exercise mimetics.

77 Eugenol contains a vanilloyl fragment that may bind to TRPV1 similarly to capsaicin,
78 implying that eugenol might exert its biological activity via TRPV1 (***Harb et al., 2019***). It has
79 been found that eugenol activates TRPV1 in a heterologous expression system and rat trigeminal
80 ganglion neurons (***Xu et al., 2006; Yang et al., 2003***). Furthermore, a recent study demonstrated
81 that eugenol activated TRPV1 in skeletal muscle (***Jiang et al., 2022***). TRPV1 is an important Ca^{2+}
82 entry pathway contributing to increase intracellular Ca^{2+} (***Nilius et al., 2007***), suggesting that
83 TRPV1 may regulate many biological processes through Ca^{2+}-dependent signaling pathways. As
84 a Ca^{2+}-dependent signaling, calcineurin (CaN) is a core signaling to promote fast to slow muscle
85 fiber transformation (***Sakuma and Yamaguchi, 2010***). Additionally, CaN signaling plays an

essential role in regulating the expression of myokine IL-6 (***Banzet et al., 2005; Banzet et al., 2007***). Therefore, we hypothesize that eugenol, as an exercise mimetic, promotes the release of myokines and fast to slow muscle fiber transformation via the TRPV1-mediated CaN signaling pathway. The primary objective of this study is to investigate this hypothesis.

Results

Eugenol promotes fast to slow muscle fiber transformation in mice and in C2C12 myotubes

As depicted in Figure 1A and B, eugenol did not have any effect on the body weight or skeletal muscle weight in mice. However, the skeletal muscle in the EUG50 and EUG100 groups exhibited a redder muscle color (Figure 1C), indicating a shift from fast to slow muscle fiber in these two groups. Further experiments showed that EUG50 and EUG100 increased the expression of slow MyHC and decreased the expression of fast MyHC protein in GAS and TA muscles (Figure 1D and E). Additionally, the mRNA expression of *MyHC I*, *MyHC IIa*, *MyHC IIx*, and *MyHC IIb* was generally consistent with protein expression (Figure 1G). As our *in vivo* studies demonstrated that the EUG200 group had no effect on muscle fiber type, we suspected that high doses of eugenol may have no impact on muscle fiber type. Therefore, we selected a broad range of eugenol doses (0-200 μM) based on the safe range of eugenol doses determined by the CCK-8 assay (Figure 1-figure supplement 1) to treat C2C12 myotubes and replicate these results *in vivo*. As indicated in Figure 1F, 12.5-50 μM eugenol boosted slow MyHC expression, while 12.5-100 μM eugenol decreased fast MyHC expression. Furthermore, as shown in Figure 1H, 100 μM eugenol increased the mRNA expression of *MyHC I*, and 12.5-100 μM eugenol increased the mRNA expression of *MyHC IIa*, whereas 50 μM eugenol decreased the mRNA expression of *MyHC IIb*. Consistent with our in vivo studies, our in vitro findings again suggested that high doses (200 μM) of eugenol had no effect on muscle fiber type. In summary, our results suggest that eugenol promotes a transformation from fast to slow muscle fiber. However, it should be noted that high doses of eugenol may have no effect on muscle fiber type.

Eugenol promotes oxidative metabolism activity, mitochondrial function, and endurance performance

An increase in the proportion of slow muscle fibers is often accompanied by an increase in skeletal muscle oxidative metabolism activity, mitochondrial function, and endurance performance. Therefore, we examined these indicators in our study. As shown in Figure 2A, EUG100 increased the exhaustion time of mice. As shown in Figure 2B, EUG50 and EUG100 decreased LDH activity and increased SDH activity in the GAS muscle. In the TA muscle, LDH activity was decreased in all EUG groups, and EUG100 increased the activities of SDH and MDH. Then, we chose 100 mg/kg eugenol (as the optimal dose) for the exhausting swimming test. In addition, the transcript levels of mitochondrial transcription factors *PGC-1α*, *NRF1*, and *TFAM* and the mRNA expression of components of the mitochondrial electron transport chain were increased in eugenol-treated mice (Figure 2C). The protein expression of mitochondrial electron transport complex I and complex V was upregulated in eugenol-treated mice (Figure 2D). Furthermore, EUG100 improved the mtDNA copy number in the GAS and TA muscle (Figure 2E), and 12.5-100 μM EUG increased the mtDNA copy number in C2C12 myotubes (Figure 2F).

Eugenol promotes lipolysis and browning of fat

Our research has found that both EUG100 and EUG200 promoted average daily feed intake (ADF) (Figure 3A). However, interestingly, there was no change in body weight (Figure 1A). This indicates that there was an increase in ADF/average daily weight gain (ADG) (Figure 3A). In addition, eugenol decreased iWAT and gWAT weight while promoting BAT weight (Figure 3B). And eugenol decreased T-CHO and LDL while increasing HDL level in serum (Figure 3C). These apparent results suggest that eugenol may increase the energy metabolism rate in mice, offsetting the weight gain and increased fat synthesis resulting from increased food intake. Therefore, we further speculate that eugenol may promote lipolysis and fat thermogenesis. As we

speculated, we found that eugenol promoted the mRNA expression of the fat synthesis-related genes *PPARγ* and *HSL*, as well as the fatty acid transport gene *FABP4*, in iWAT (Figure 3D). In gWAT, it was found that eugenol promoted the mRNA expression of the *FASN* and *FABP4* (Figure 3D). We further examined the mRNA expression of key genes involved in browning of fat, and found that eugenol promoted the mRNA expression of *CD137*, *TBX1*, *UCP-1*, *PRDM16*, *Dio2*, and *Cidea* in iWAT, while eugenol promoted the mRNA expression of *TMEM26*, *UCP-1*, *PRDM16*, *Dio2*, and *Cidea* in gWAT (Figure 3E). At the protein level, eugenol promoted the expression of the fatty acid transport protein FABP-1, as well as the UCP-1 protein expression in gWAT (Figure 3F). In addition, we also examined the effects of eugenol on the browning-related proteins and mitochondrial complex proteins in BAT. It was found that eugenol promoted the UCP-1 and PGC-1α protein expression (Figure 3G), as well as the mitochondrial electron transport complex III and complex V protein expression (Figure 3H). Together, these results indicate that eugenol promotes lipolysis and browning of fat.

Eugenol activates TRPV1-mediated CaN/NFATc1 signaling pathway in skeletal muscle

Based on the gene expression profiling, it was observed that TRPV1 is expressed in all tissues, including adipose and muscle tissues, with the highest expression in skeletal muscle compared to other TRP channels (Figure 4A and Figure 4-figure supplement 1A). qPCR analysis confirmed the expression of TRPV1 and TRPV2 in skeletal muscle, and the mRNA expression of only *TRPV1* was promoted by EUG50 and EUG100 in TA muscle. In C2C12 cells, only TRPV1-4 were expressed, and only *TRPV1* mRNA expression was promoted by 25 and 50 μM eugenol (Figure 4C). Adipose tissue expressed TRPV1 and TRPV2 genes, and EUG100 and EUG200 promoted *TRPV1* mRNA expression, while EUG50 promoted T*RPV2* mRNA expression (Figure 4-figure supplement 1B and C). The effect of eugenol on TRPV1 protein expression was consistent with its effect on *TRPV1* mRNA expression in both skeletal muscle tissue and C2C12 cells (Figure 4D-F). Moreover, taking the TRPV1-capsaicin binding sites (TYR511, SER512,

THR550, and GLU570) (***Carnevale and Rohacs, 2016***) as the potential binding pocket, molecular docking analysis showed that eugenol bound at the binding pocket and interacted with THR550, ASN551, LEU553, TYR554, ALA566, ILE569, GLU570, and ILE573 (Figure 4-figure supplement 2). Based on the above results, we conclude that eugenol has the potential to activate TRPV1 in both skeletal muscle and adipose tissue. We further investigated the TRPV1-mediated CaN/NFATc1 signaling pathway in skeletal muscle. CnA is a catalytic subunit of CaN, and its expression level reflects the activity of CaN. Our results showed that EUG50 and EUG100 increased CnA protein expression in the GAS and TA muscles (Figure 4D and 4E), and 12.5-100 μM eugenol promoted CnA protein expression in C2C12 myotubes (Figure 4F). The regulator of calcineurin 1 (MCIP1) is a biomarker to reflect the CaN activity (***Yang et al., 2000***), the mRNA expression of *MCIP1* was increased in EUG100 groups (Figure 4-figure supplement 3). Furthermore, the nuclear translocation of NFATc1 was promoted by EUG50 and EUG100 in the GAS and TA muscles, and by 12.5-50 μM eugenol in C2C12 myotubes (Figure 4G-I). In summary, our *in vivo* and *in vitro* studies both suggest that eugenol can activate the TRPV1-mediated CaN/NFATc1 signaling pathway in skeletal muscle. Interestingly, similar to the effects of eugenol on muscle fiber types, we again found that high doses of eugenol have no effect on the signaling pathway.

Eugenol promotes fast to slow muscle fiber transformation by activating TRPV1-mediated CaN/NFATc1 signaling pathway

To further investigate the role of TRPV1 in regulating fast to slow muscle fibers, we treated C2C12 myotubes with 25 μM eugenol and either 1 μM TRPV1 inhibitor AMG-517 or 0.5 μM CaN inhibitor cyclosporine A (CsA). The results showed that TRPV1 inhibition weakened the increase in intracellular Ca^{2+} levels induced by eugenol, suggesting that eugenol acts via TRPV1 (Figure 5A). Furthermore, the inhibition of TRPV1 and CaN attenuated the effect of eugenol on CaN (Figure 5B). In addition, eugenol increased the mitochondrial electron transport complex I,

II, III, and V protein expression, the inhibition of TRPV1 and CaN attenuated the effect of eugenol on complex I, III, and V (Figure 5C). Importantly, immunofluorescence and Western blot analysis revealed that eugenol promoted the fast to slow muscle fiber transformation, while the inhibition of TRPV1 and CaN eliminated this effect (Figure 5D and Figure 5E).

The myokines regulated by CaN

To investigate which myokines are controlled by CaN, C2C12 myotubes were treated with the Ca^{2+} ionophore A23187. As shown in Figure 6A-C, A23187 increased the mRNA expression of *MCIP1*, the protein expression of CnA, and CaN activity. We chose 0.5 μM A23187 for subsequent experiments and confirmed that it increased intracellular Ca^{2+} levels (Figure 6D). To identify CaN-controlled myokines, we next detected the mRNA expression of several myokines that have been well documented to improve metabolic homeostasis (***Eckel, 2019; Whitham and Febbraio, 2016***) and promote fast to slow muscle fiber transformation (***Correia et al., 2021; Knudsen et al., 2020; Men et al., 2021; Quinn et al., 2013***) (Table1). As shown in Figure 6E, A23187 significantly increased the mRNA expression of *FNDC5*, *IL-6*, *IL-15*, and *Metrnl*. However, *IL-13* mRNA expression was not detected in C2C12 myotubes. In addition, a correlation heatmap showed the highest correlation coefficient (R=0.954) between MCIP1 expression and IL-15 expression, followed by MCIP1 and IL-6 (R=0.846), MCIP1 and Metrnl (0.77), and MCIP1 and FNDC5 (0.651) (Figure 6F). Furthermore, a TFBS prediction revealed more potential binding sites between the IL-15 promoter and NFATc1 (Figure 6G). Based on the correlation and TFBS analysis, it was suggested that IL-15 is the myokine most likely to be regulated by the CaN/NFATc1 signaling pathway, and we selected it for further study.

The myokine IL-15 expression depends on CaN/NFATc1 signaling pathway

Firstly, it was observed that treatment with 0.5 and 1 μM Ca^{2+} ionophore led to upregulation of IL-15 protein expression (Figure 7A). Subsequently, we treated C2C12 myotubes with 0.5 μM Ca^{2+} ionophore and 0.5 μM CsA to investigate their effects. We found that Ca^{2+} ionophore

treatment upregulated the expression of CnA, NFATc1, and IL-15 proteins, while inhibition of CaN eliminated these effects (Figure 7B-D). Furthermore, Ca^{2+} ionophore treatment increased the expression of slow MyHC and decreased the expresssion of fast MyHC, while CsA blocked this effect (Figure 7-figure supplement 1). Based on the transcription factor motif databases (JASPAR and hIFtarget), it was predicted that a sequence (5'-AATGGAAAA-3') in the promoter regions of IL-15 was a potential binding site of NFATc1 (Figure 7E), and DNA-protein docking analysis also revealed a high probability of binding between this sequence and the NFATc1 protein (Figure 7F). We then performed an EMSA assay to validate the binding of NFATc1 to this sequence. The probes used in the EMSA assay were shown in Figure 7G and the EMSA results were shown in Figure 7H. We observed upward migration bands when the C2C12 nuclear protein extract (NE) was incubated with the bio-NFATc1 probe (lanes 2-4), and compared to the control (lane 2) and CsA inhibition group (lane 4), Ca^{2+} treatment group showed higher expression of the band (lane 3). Moreover, the use of competing cold-NFATc1 probes showed no upward migration band (lane 5), while using the mut-NFATc1 probe again showed the band (lane 6). These findings suggest that NFATc1 may bind to the promoter of IL-15. We further investigated whether NFATc1 transcriptionally activates IL-15 through luciferase reporter assays. As shown in Figure 7I, overexpression of NFATc1 promoted NFATc1 protein expression in HEK293T cells. Additionally, after transfection with the IL-15 reporter plasmid, overexpression of NFATc1 enhanced the relative fluorescence intensity (Figure 7J), suggesting that the transcriptional activation of IL-15 is regulated by NFATc1.

Eugenol promotes IL-15 level by TRPV1-mediated CaN/NFATc1 signaling pathway

We conducted further experiments to examine the effect of eugenol on IL-15 expression. Our results (Figure 8A-C) showed that EUG50 and EUG100 promoted the mRNA and protein expression of IL-15 in both GAS and TA muscle. Interestingly, in EDL and SOL muscle, which are dominated by fast and slow muscle fibers respectively, EUG100 promoted IL-15 mRNA

expression (Figure 8D). We also found that the mRNA expression of IL-15 was higher in SOL muscle than in EDL muscle (Figure 8D). Moreover, Pearson's correlation analysis showed that IL-15 expression positively correlated with MyHC I (R=0.714) and MyHC IIa (R=0.774) expression, and negatively correlated with MyHC IIb (R=-0.568) (Figure 8D). Consistent with the mRNA expression data, the IL-15 protein expression was also higher in SOL muscle than in EDL muscle (Figure 8E). Additionally, EUG50 and EUG100 increased the concentration of IL-15 in the serum (Figure 8F). These findings suggested that IL-15 was a oxidative muscle fiber type-specific myokine that was promoted by eugenol. Our in vitro experiments showed that 25 and 50 μM eugenol increased the mRNA expression and secretion of IL-15 (Figure 9A and B), which was consistent with our in vivo experiments. In addition, the inhibition of TRPV1 and CaN decreased the upregulation of eugenol on IL-15 mRNA and protein expression (Figure 9C and D). Immunofluorescence staining with IL-15 also showed similar results (Figure 9-figure supplement 1).

Discussion

Our study reveals that eugenol can serve as an exercise mimetic that promotes remodeling of skeletal muscle fibers and expression of the myokine IL-15 through the TRPV1-mediated CaN/NFATc1 signaling pathway. This expands the traditional biological functions of eugenol and provides a theoretical basis for its potential applications in the food and drug industry. Moreover, we identify a novel TRPV1-mediated CaN/NFATc1 signaling pathway that promotes the transformation of fast to slow muscle fibers. Importantly, we provide the first explanation of the mechanism underlying the release of the myokine IL-15.

TRPV1, like all other TRP channels, assembles as tetramers to form cation-permeable pores (***Clapham, 2003***). Initially identified as a capsaicin receptor and heat-activated ion channel that modulates pain and neurogenic inflammation (***Caterina et al., 1997***), subsequent studies have found that TRPV1 is expressed on many non-neural sites and plays roles in immunity,

vasculature, obesity, and thermogenesis (***Fernandes et al., 2012***). Previous studies have also shown that capsaicin activated TRPV1 to improve endurance capacity and energy metabolism (***Luo et al., 2012***), counter obesity (***Baskaran et al., 2016***), and intervene diabetes (***Wang et al., 2012***). Therefore, TRPV1 is a strong target for the discovery of exercise mimetics, which drove us to search for TRPV1 agonists that may act as exercise mimetics. We focused on eugenol, a healthy and edible plant extract that may be a potential TRPV1 agonist. Since eugenol contains a vanilloyl fragment, it is possible to bind TRPV1 through a similar pattern to capsaicin. Indeed, previous studies have found that eugenol activates TRPV1 in a heterologous expression system and rat trigeminal ganglion neurons (***Xu et al., 2006; Yang et al., 2003***), and a recent study reported that 50 and 100 μM eugenol promoted TRPV1 expression in C2C12 myotubes (***Jiang et al., 2022***). In our study, we investigated the mRNA expression profile of TRP channels in C2C12 myotubes and skeletal muscle, and found that only TRPV1 mRNA was upregulated in response to eugenol treatment. Moreover, it was observed that the protein expression of TRPV1 was consistent with the mRNA expression. Our molecular docking results also indicated that eugenol bound to the capsaicin binding pockets of TRPV1. Based on these findings, we propose that eugenol specifically activates TRPV1 in skeletal muscle, rather than other TRP channels. This may be due to the relatively higher expression of TRPV1 in skeletal muscle compared to other TRP channels.

One of the benefits of exercise mimetics for body is to promote the skeletal muscle oxidative phenotype and endurance performance (***Fan and Evans, 2017***). Our studies showed that eugenol improved endurance performance and promoted fast-to-slow muscle fiber transformation. Slow muscle fibers are characterized by the improvement in mitochondrial function and oxidative metabolism (***Choi and Kim, 2009***). As expected, eugenol also promoted mitochondrial function and oxidative metabolism capacity in skeletal muscle. In a previous study, capsaicin-induced TRPV1 activation was shown to promote exercise endurance and the skeletal muscle oxidative

286 phenotype (***Wang et al., 2012***). The authors suggested that TRPV1 activated calmodulin-
287 dependent protein kinase (CaMK) by increasing intracellular Ca^{2+}, and the activation of CaMK
288 further activated PGC-1α, contributing to these effects (***Wang et al., 2012***). In skeletal muscle, the
289 CaN signaling pathway is also an important Ca^{2+}-mediated signal that promotes the muscle
290 oxidative phenotype (***Sakuma and Yamaguchi, 2010***). CaN induces the translocation of NFATc1
291 to the nucleus by dephosphorylating NFATc1, thereby switching fast to slow muscle fibers
292 (***Calabria et al., 2009***). TRPV1 activation has been shown to promote CaN activity in several
293 other cells and tissues (***Hou et al., 2019; Ma et al., 2011; Yang et al., 2018***), but the link between
294 TRPV1 and CaN signaling in skeletal muscle has not yet been established, nor has it been
295 determined whether TRPV1 promotes muscle oxidative phenotype through the CaN/NFATc1
296 signaling pathway. Therefore, we investigated the role of TRPV1-mediated CaN signaling
297 pathway in the regulation of muscle fiber types. We found that eugenol increased CaN expression
298 through the activation of TRPV1, and that it promoted fast-to-slow muscle fiber transformation
299 via the TRPV1-mediated CaN/NFATc1 signaling pathway. Recent studies have also found that
300 eugenol increases muscle glucose uptake through the TRPV1/CaMK signaling pathway (***Jiang et***
301 ***al., 2022***), suggesting that both CaN and CaMK signaling may be involved in TRPV1-facilitated
302 skeletal muscle oxidative phenotype.

303 Another benefit of exercise mimetics is the alleviation of obesity and improvement of
304 metabolic health. It has been reported that an increase in slow-twitch fiber content is positively
305 associated with reduced obesity and improved metabolic health (***Carlson et al., 2010***). Previous
306 studies have shown that eugenol can reduce blood lipids in rats with hyperlipidemia (***Harb et al.,***
307 ***2019***), lower blood glucose and insulin resistance in diabetic mice (***Al-Trad et al., 2019; Sanae et***
308 ***al., 2014***), and reduce hepatic lipid accumulation in high-fat-fed mice (***Rodrigues et al., 2022***),
309 demonstrating its potential in improving glucose and lipid metabolism. In our study, we found
310 that feeding eugenol under standard diet conditions may promote fat thermogenesis and browning

311 to facilitate fat breakdown. Interestingly, it was found that capsaicin alleviated obesity and
312 promoted white fat browning by activating the TRPV1 (***Baskaran et al., 2016***). Our study found
313 that eugenol promoted TRPV1 mRNA expression in adipose tissue, indicating that eugenol may
314 promote white fat browning through TRPV1 activation.

315 Exercise mimetics may exert beneficial effects on the body by promoting the release of
316 myokines (***Fan and Evans, 2017***). Some myokines, such as IL-13 (***Knudsen et al., 2020***), IL-15
317 (***Quinn et al., 2013***), and neurturin (***Correia et al., 2021***), have been well documented to improve
318 metabolic homeostasis, promote fast to slow muscle fiber transformation, and improve endurance
319 capacity. However, the regulatory mechanisms for myokines expression are largely unclear. Since
320 myokines are usually promoted by muscle contraction, and Ca^{2+} is the main signal in muscle
321 contraction, CaN, downstream of Ca^{2+}, has been considered to regulate myokine expression. CaN
322 has been reported to regulate the expression of myokine IL-6 (***Banzet et al., 2005; Banzet et al.,***
323 ***2007***). Additionally, the transcriptional activation activity of myokines IL-4 and IL-13 is thought
324 to be promoted by transcription factor NFATc2, which is downstream of CaN (***Jacquemin et al.,***
325 ***2007; Zádor, 2008***). Based on the correlation and TFBS analysis, it was found that IL-15 is most
326 likely to be regulated by the CaN/NFATc1 signaling pathway in our study. IL-15 has been
327 reported as a myokine that improves fatty acid utilization, insulin sensitivity, and endurance
328 capacity, and prevents obesity and diabetes (***Nadeau and Aguer, 2019***). In different cell models,
329 CsA-mediated inhibition of CaN decreased the release of IL-15 (***Cho et al., 2002; Cho et al.,***
330 ***2007***). Furthermore, an increase in CaN expression in 3T3-L1 cells was accompanied by an
331 increase in IL-15 expression (***Almendro et al., 2009***). Our study found that the CaN/NFATc1
332 signaling pathway contributes to the eugenol-promoted expression of IL-15. Furthermore, we
333 observed that the expression of IL-15 was higher in the slow-twitch SOL muscle than in the fast-
334 twitch EDL muscle, suggesting that an increase in muscle oxidative phenotype may further

promote the release of IL-15. However, the mechanism underlying how IL-15 promotes the muscle oxidative phenotype remains unclear and requires further investigation.

Apparently, an interesting finding throughout our *in vitro* and *in vivo* study was that the high doses of eugenol (200 mg/kg for mice and 200 μM eugenol for C2C12 myotubes) had no effect on TRPV1-mediated CaN/NFATc1 signaling pathway, IL-15 expression, and muscle fiber type. We suspected that high doses of eugenol may cause desensitization of TRPV1 in skeletal muscle under our study conditions. This indirectly verified that the activation of TRPV1 does promote IL-15 expression and fast-to-slow muscle fiber transformation type. It is well-known that continuous activation of TRPV1 by capsaicin causes TRPV1 desensitization, which is considered to underlie the analgesic effects of capsaicin (***Koplas et al., 1997***). As previously reported, TRPV1 agonists promoted TRPV1 desensitization in a dose- and time-dependent manner by targeting lysosomes to degrade TRPV1 in HEK293 cells (***Sanz-Salvador et al., 2012***). A hypothetical model suggested that upon TRPV1 opening to allow Ca^{2+} influx, Ca^{2+}/CaM binds to the CaM-binding domain of TRPV1, leading to channel inactivation, and CaN dephosphorylates TRPV1 to desensitize TRPV1 (***Hasan and Zhang, 2018***). However, most results on TRPV1 desensitization were obtained by capsaicin treatment of cells, and it is unknown whether high-dose eugenol promotes TRPV1 desensitization through a similar mechanism. Therefore, it is essential to select the appropriate dose of eugenol for the application of TRPV1 activators.

In conclusion, our findings indicate that eugenol can promote the transformation of fast to slow muscle fibers and induce the myokine IL-15 expression through the TRPV1-mediated CaN/NFATc1 signaling pathway. Moreover, our study is the first to demonstrate that the expression of IL-15 is regulated by the CaN/NFATc1 signaling pathway. These results suggest that eugenol may have potential as a novel exercise mimetic and that TRPV1 may represent a promising therapeutic target for metabolic disorders.

Methods and Materials

Animals, treatments, and sample collection

A total of eighty 4-week-old male C57BL/6J mice (Dashuo Experimental Animal Co.Ltd., Chengdu, China) were divided into four treatments (n = 12) using a simple randomization method. The control group were fed a basal diet supplemented with 0% eugenol (EUG, purity≥98%, Sigma, St. Louis, MO, USA), other groups were fed a basal diet supplemented with 50, 100 and 200 mg/kg eugenol, respectively (EUG50, EUG100 and EUG200). All mice were housed in individual cages (23°C ± 2°C, 12-h light/12-h dark cycle) and provided with free access to feed and water. The experiment lasted for 4 weeks. The weight of mice was measured every week. At the end of the experiment, mice anesthetized with CO_2 were sacrificed. After being weighed and photographed, skeletal muscle [including tibialisanterior (TA), gastrocnemius (GAS), soleus (SOL), and extensor digitorum longus (EDL)], fat [including inguinal white adipose tissue (iWAT), gonadal white adipose tissue (gWAT), brown adipose tissue (BAT)] were collected and stored at -80 °C for subsequent analyses. All procedures of animal experiments were performed according to protocols approved the Animal Care Advisory Committee of Sichuan Agricultural University under permit No. YYS20200929.

Exhausting swimming test

The forced swimming capacity test was employed in this study to evaluate the effects of eugenol on endurance capacity in mice. A total of thirty 4-week-old mice were divided into the control and EUG100 group (n=15). After four weeks of feeding, the mice with a load of lead wire (7% of body weight) attached to its tail were placed in individual swimming pools (25 ± 1°C, 35-cm depth). Exhaustive swimming time was immediately recorded when the mice failed to return to the surface continuously over a 7-second time frame and showed a lack of coordinated movements.

Cell culture and treatments

384 C2C12 cells (Shanghai Cell Bank, Chinese Academy of Sciences, passages 3-8) were
385 cultured in Dulbecco modified Eagle medium (DMEM) (Invitrogen, Carlsbad, CA, USA)
386 supplemented with 10% fetal bovine serum (Gibco, Paisley, Scotland, UK), 100 mg/L
387 streptomycin and 100 U/ml penicillin (Gibco) at 37°C in a 5 % CO2 atmosphere. When cells
388 reached ~80% confluence, 2% horse serum (Gibco) replaced 10% fetal bovine serum to induce
389 differentiation. For eugenol treatment, cells were treated with 0, 12.5, 25, 50, 100, 200 μM EUG
390 for 1 day after 4 days of differentiation. For Ca^{2+} ionophore A23187 (Sigma) treatment, cells were
391 treated with 0, 0.1, 0.5, 1 μM A23187 for 16 h after 2 days of differentiation, or cells were treated
392 with 0.5 μM A23187 and 0.5 μM CsA. For the following mechanism studies, cells were treated
393 with 25 μM EUG and 1 μM TRPV1 inhibitor AMG-517 or 0.5 μM CaN inhibitor cyclosporin A
394 (CsA, Sigma).

395 *Cell viability assay*

396 Cell viability was analyzed using Cell-Counting Kit-8 (Beyotime, Jiangsu, China) to
397 determine the safe dose of EUG on C2C12 myotubes. Briefly, cells were treated with EUG (0,
398 12.5, 25, 50, 100, 200, 400, 800, 1600 μM) for 1 day after 4 days of differentiation, 10 μL CCK-8
399 solution was then added to each well and then incubated for 1 h at 37 ℃. After incubation, the
400 OD value was immediately measured at 450 nm using the SpectraMax 190 Absorbance Plate
401 Reader.

402 *Measurement of intracellular calcium ion (Ca^{2+})*

403 After 1 day of treatment with C2C12 myotubes in 24-well cell culture plates, the cells were
404 digested using Trypsin-EDTA solution and transferred from each well into a centrifuge tube. The
405 Trypsin-EDTA solution was removed and the cells were washed 3 times with a calcium-free PBS
406 solution. Following this, the PBS solution was removed and 200 μL of 5 μM Ca^{2+} fluorescent
407 probe Fluo-4 (Beyotime) was added to the cells and incubated at 37°C for 30 minutes. After the
408 incubation, the probe was removed by washing the cells 3 times with PBS. Finally, Ca^{2+}

409 fluorescence was detected using flow cytometry (FACSVerse, BD Biosciences, East Rutherford,
410 NJ, USA) and analyzed using FlowJo 10.0.7 software.

411 *Gene expression and mitochondrial DNA quantitative PCR (qPCR)*

412 Total RNA was extracted using RNA isolater Total RNA Extraction Reagent (Vazyme,
413 Nanjing, China) and genomic DNA was extracted using mammalian genomic DNA extraction kit
414 (Beyotime) according to the instructions. After measuring the concentration of total RNA, total
415 RNA reverse transcribed to cDNA using HiScript II Q RT Supermix (Vazyme). qPCR was
416 performed using ChamQ SYBR Color qPCR Master Mix (Vazyme) on a 7900 HT Real-time PCR
417 system (384-cell standard block) (Applied Biosystems). Relative mtDNA was quantified by qPCR
418 using primers for mitochondrially-encoded *Nd1* normalized to nuclear-encoded *36B4 (Rplp0)*
419 DNA. And *GAPDH* was used as an endogenous control for normal qPCR. The primer sequences
420 are listed in Appendix 1—table 1.

421 *Protein extraction and Western Blot*

422 RIPA lysis buffer (Beyotime) was used to extract total protein. The nuclear protein was
423 extracted using NE-PER Nuclear and Cytoplasmic Extraction Reagents (ThermoFisher). Protein
424 from conditioned media was extracted using methanol-choloroform precipitation method as
425 previous (***Jakobs et al., 2013***). Protein concentration was determined by the BCA assays, and then
426 proteins were transferred to a nitrocellulose membrane using a wet Trans-Blot system (Bio-Rad,
427 Hercules, CA, USA). The primary antibodies used were anti-slow MyHC (Sigma, cat. no.
428 M8421), anti-fast MyHC (Sigma, cat. no. M4276), anti-TRPV1 (Alomone, cat. no. ACC030),
429 anti-Calcineurin A (CnA, abcam, cat. no. ab90540), anti-NFATc1 (Cell Signaling Technology, cat.
430 no. #8032), anti-IL-15 (R&D system, cat. no. AF447), anti-PGC-1α (Proteintech, cat. no. 66369-
431 1-Ig). anti-NDUFA9 (GeneTex, cat. no. GTX132978), anti-SDHA (GeneTex, cat. no.
432 GTX636098), anti-UQCRC1 (GeneTex, cat. no. GTX630393), anti-MTCO1(Bioss, cat. no. bs-
433 3953R), anti-ATP5B (GeneTex, cat. no. GTX132925), anti-FABP1 (Cell Signaling Technology,

434 cat. no. #13368), anti-UCP-1 (Proteintech, Cat. no. 23673-1-AP), anti-PRDM16 (R&D system,
435 cat. no. AF6295), anti-β-actin (TransGen, cat. no. HC201-01), and anti-Histone H3 (Beyotime,
436 cat. no. AF0009). Coomassie staining is depicted as loading control for conditioned media protein
437 (***Welinder and Ekblad, 2011***). The signal was visualized using a Clarity Western ECL Substrate
438 (BioRad, Hercules, CA, USA) and a ChemiDoc XRS Imager System (BioRad). The target band
439 density was identified using Image Lab 5.1 (BioRad).

440 *Immunofluorescence (IF)*

441 After treatment, C2C12 myotubes were washed three times (5 min each time) with
442 phosphate-buffered saline (PBS) and fixed in Immunol Staining Fix Solution (Beyotime) for 20
443 min. Then C2C12 myotubes were permeabilized with 0.5% Triton X-100 for 20 min, blocked
444 with blocking buffer for 2 hours at 37 ℃, incubated with the primary antibodies including slow
445 MyHC (1:50, Sigma, Cat. No. M8421) for 16 hours, and incubated with the fluorescent secondary
446 antibody (1:1000, Cell Signaling, USA) for 2 hours at 37 ℃. Finally, 4,6-diamidino-2-
447 phenylindole (DAPI) (Beyotime) was used to stain cell nucleus for 10 minutes at room
448 temperature. A positive signal was detected and captured using fluorescence microscopy (Lecia
449 DMI4000 B).

450 *Molecular-protein docking and DNA-protein docking*

451 The protein structures of TRPV1 (PDB codes: 5IS0) and NFATc1 (PDB codes: 1A66) were
452 downloaded from the Research Collaboratory for Structural Bioinformatics Protein Data Bank
453 database (RCSB PDB, https ://www.rcsb.org/) (***Burley et al., 2019***). The structure of eugenol
454 (ZINC1411) was downloaded from the ZINC database (https://zinc.docking.org/substances/). The
455 DNA structure was generated using Discovery Studio 2019 software (Discovery Studio 2019;
456 BIOVIA; San Diego, USA). Discovery studio 2019 software was used to perform molecular-
457 protein docking. HDOCK (http://hdock.phys.hust.edu.cn/) was used to perform DNA-protein
458 docking.

Prediction of transcription factors binding sites (TFBS)

The gene promoter sequences of mouse (upstream 2 kb) were acquired from National Center for Biotechnology Information. hIFtarget (http://bioinfo.life.hust.edu.cn/hTFtarget#!/) and JASPAR (http://jaspar.ge-nereg.net/) applied to predict the potential NFATc1 binding sites at the promoter of genes. A putative binding sites predicted by both two tools were selected for further electrophoretic mobility shift (EMSA) probes design.

Electrophoretic mobility shift assay (EMSA)

After synthesizing the single-stranded probes for EMSA, annealing buffer for DNA oligos (5x) (Beyotime) was used to anneal to form double-stranded DNA probes. EMSA assay were performed using chemiluminescent EMSA Kit (Beyotime) according to the instructions. Briefly, 10 μL reaction system with nuclease-free water, EMSA/Gel-Shift Binding Buffer, nuclear protein, and probe was transferred to a nitrocellulose membrane using a wet Trans-Blot system. The reaction system includes negative control reaction (no nuclear protein), sample reaction, probe cold competition reaction (100-fold unlabeled probe), mutation probe cold competition reaction (100-fold unlabeled mutation probe). The signal was visualized using a Clarity Western ECL Substrate (BioRad, Hercules, CA, USA) and a ChemiDoc XRS Imager System (BioRad).

Plasmid construction and extraction

The plasmid of pcDNA3.1 vector, pCDNA3.1-NFATc1 (The NFATc1 coding sequences were inserted into the pcDNA3.1 vector), pGL3 vector, and pGL3-IL15 (The sequence of 2 kb upstream of the IL-15 promoter sequence were inserted into the pGL3 vector) were from Tsingke Biotechnology Co., Ltd (Beijing, China). Plasmid amplification is provided in *Escherichia coli* bacteria cells. Plasmid Maxi Preparation Kit for All Purpose (Beyotime) was used to extract plasmids.

Dual-luciferase reporter gene assay

HEK293T cells in 48-well plates were transfected with pcDNA3.1 together with pGL3 or pcDNA3.1-NFATc1 together with pGL3 or pcDNA3.1 together with pGL3-IL15 or pcDNA3.1-NFATC1 together with pGL3-IL15. Luciferase activity was detected by a Dual-Luciferase assay kit (Beyotime) with Glomax 96 microplate luminometer (Promega) in luminometer mode. The raw values of firefly luciferase were normalized to Renilla luciferase.

Enzyme activities analysis

The tissue and C2C12 myotube were homogenized in saline and centrifuged at 3500 × g 4 ℃ for 10 minutes. The supernatant was carefully transferred to a centrifuge tube. Total protein concentration was determined by the BCA assays. The enzyme activity of lactate dehydrogenase (LDH), malate dehydrogenase (MDH), succinic dehydrogenase (SDH), and CaN were measured using commercial assay kits (Nanjing Jiancheng Bioengineering Institute, Nanjing, China).

Statistical analyses

SAS 9.4 software was used to perform one-way ANOVA and t test. After the normality and homogeneity test, one-way ANOVA followed by Duncan's multiple range test was performed for multiple-groups comparisons. Student's t test was performed for two-groups comparisons. Correlation analysis was performed by Pearson's correlation coefficient analysis. Statistical methods were not used to predetermine sample size. GraphPad Prism 8.0 (GraphPad Software, Inc., San Diego, CA) software was used to draw column charts and Omicstudio tools (https://www.omicstudio.cn/tool.) was used to draw heatmaps. Data were expressed as mean ± SEM. Statistical significance was defined as $^{\#}P < 0.1$, $^{*}P < 0.05$, $^{**}P < 0.01$, and $^{***}P < 0.001$ for all figures.

Author contributions

Tengteng Huang: Investigation, Data curation, Formal analysis, Writing - original draft. Xiaoling Chen: Conceptualization, Methodology, Project administration, Supervision. Jun He:

Methodology. Ping Zheng: Methodology. Yuheng Luo: Methodology. Aimin Wu: Methodology. Hui Yan: Methodology. Bing Yu: Methodology. Daiwen Chen: Methodology. Zhiqing Huang: Conceptualization, Funding acquisition, Methodology, Supervision, Writing - review & editing

Competing interests

The authors declare no competing interest.

Data availability

Data will be made available on request.

Funding

This work was supported by the National Key R&D Program of China (No. 2023YFD1301302), the National Natural Science Foundation of China (No. 32372901), the Natural Science Foundation of Sichuan Province (No. 2023NSFSC0238), and the Sichuan Science and Technology Program (No. 2021ZDZX0009).

References

Almendro V, Fuster G, Ametller E, Costelli P, Pilla F, Busquets S, Figueras M, Argilés JM, López-Soriano FJ. 2009. Interleukin-15 increases calcineurin expression in 3T3-L1 cells: possible involvement on in vivo adipocyte differentiation. *International Journal of Molecular Medicine* **24**:453–458. doi: 10.3892/ijmm_00000252.

Al-Trad B, Alkhateeb H, Alsmadi W, Al-Zoubi M. 2019. Eugenol ameliorates insulin resistance, oxidative stress and inflammation in high fat-diet/streptozotocin-induced diabetic rat. *Life Sciences* **216**:183–188. doi: 10.1016/j.lfs.2018.11.034.

Banzet S, Koulmann N, Sanchez H, Serrurier B, Peinnequin A, Alonso A, Bigard X. 2007. Contraction-induced interleukin-6 transcription in rat slow-type muscle is partly dependent

on calcineurin activation. *Journal of Cellular Physiology* **210**:596–601. doi: 10.1002/jcp.20854.

Banzet S, Koulmann N, Simler N, Birot O, Sanchez H, Chapot R, Peinnequin A, Bigard X. 2005. Fibre-type specificity of interleukin-6 gene transcription during muscle contraction in rat: association with calcineurin activity. *The Journal of Physiology* **566**:839–847. doi: 10.1113/jphysiol.2005.089193.

Baskaran P, Krishnan V, Ren J, Thyagarajan B. 2016. Capsaicin induces browning of white adipose tissue and counters obesity by activating TRPV1 channel-dependent mechanisms. *British Journal of Pharmacology* **173**:2369–2389. doi: 10.1111/bph.13514.

Burley SK, Berman HM, Bhikadiya C, Bi C, Chen L, Di Costanzo L, Christie C, Dalenberg K, Duarte JM, Dutta S, Feng Z, Ghosh S, Goodsell DS, Green RK, Guranovic V, Guzenko D, Hudson BP, Kalro T, Liang Y, Lowe R, Namkoong H, Peisach E, Periskova I, Prlic A, Randle C, Rose A, Rose P, Sala R, Sekharan M, Shao C, Tan L, Tao Y-P, Valasatava Y, Voigt M, Westbrook J, Woo J, Yang H, Young J, Zhuravleva M, Zardecki C. 2019. RCSB Protein Data Bank: biological macromolecular structures enabling research and education in fundamental biology, biomedicine, biotechnology and energy. *Nucleic Acids Research* **47**:D464-D474. doi: 10.1093/nar/gky1004.

Calabria E, Ciciliot S, Moretti I, Garcia M, Picard A, Dyar KA, Pallafacchina G, Tothova J, Schiaffino S, Murgia M. 2009. NFAT isoforms control activity-dependent muscle fiber type specification. *Proceedings of the National Academy of Sciences of the United States of America* **106**:13335–13340. doi: 10.1073/pnas.0812911106.

Carlson SA, Fulton JE, Schoenborn CA, Loustalot F. 2010. rend and prevalence estimates based on the 2008 physical activity guidelines for Americans. *American Journal of Preventive Medicine* **39**:305–313. doi: 10.1016/j.amepre.2010.06.006.

Carnevale V, Rohacs T. 2016. TRPV1: A target for rational drug design. *Pharmaceuticals* **9**. doi: 10.3390/ph9030052.

Caterina MJ, Schumacher MA, Tominaga M, Rosen TA, Levine JD, Julius D. 1997. The capsaicin receptor: a heat-activated ion channel in the pain pathway. *Nature* **389**:816–824. doi: 10.1038/39807.

Cho M-L, Ju JH, Kim K-W, Moon Y-M, Lee S-Y, Min S-Y, Cho Y-G, Kim H-S, Park K-S, Yoon C-H, Lee SH, Park S-H, Kim H-Y. 2007. Cyclosporine A inhibits IL-15-induced IL-17 production in CD4+ T cells via down-regulation of PI3K/Akt and NF-kappaB. *Immunology Letters* **108**:88–96. doi: 10.1016/j.imlet.2006.11.001.

Cho M-L, Kim W-U, Min S-Y, Min D-J, Min J-K, Lee S-H, Park S-H, Cho C-S, Kim H-Y. 2002. Cyclosporine differentially regulates interleukin-10, interleukin-15, and tumor necrosis factor ? production by rheumatoid synoviocytes. *Arthritis & Rheumatism* **46**:42–51. doi: 10.1002/1529-0131(200201)46:1<42::AID-ART10026>3.0.CO;2-A.

Choi YM, Kim BC. 2009. Muscle fiber characteristics, myofibrillar protein isoforms, and meat quality. *Livestock Science* **122**:105–118. doi: 10.1016/j.livsci.2008.08.015.

Clapham DE. 2003. TRP channels as cellular sensors. *Nature* **426**:517–524. doi: 10.1038/nature02196.

Correia JC, Kelahmetoglu Y, Jannig PR, Schweingruber C, Shvaikovskaya D, Zhengye L, Cervenka I, Khan N, Stec M, Oliveira M, Nijssen J, Martínez-Redondo V, Ducommun S, Azzolini M, Lanner JT, Kleiner S, Hedlund E, Ruas JL. 2021. Muscle-secreted neurturin couples myofiber oxidative metabolism and slow motor neuron identity. *Cell Metabolism* **33**:2215-2230.e8. doi: 10.1016/j.cmet.2021.09.003.

Devi KP, Nisha SA, Sakthivel R, Pandian SK. 2010. Eugenol (an essential oil of clove) acts as an antibacterial agent against Salmonella typhi by disrupting the cellular membrane. *Journal of Ethnopharmacology* **130**:107–115. doi: 10.1016/j.jep.2010.04.025.

Duan Y, Li F, Tan B, Yao K, Yin Y. 2017. Metabolic control of myofibers: promising therapeutic target for obesity and type 2 diabetes. *Obesity Reviews* **18**:647–659. doi: 10.1111/obr.12530.

Eckel J. 2019. Myokines in metabolic homeostasis and diabetes. *Diabetologia* **62**:1523–1528. doi: 10.1007/s00125-019-4927-9.

Egan B, Zierath JR. 2013. Exercise metabolism and the molecular regulation of skeletal muscle adaptation. *Cell Metabolism* **17**:162–184. doi: 10.1016/j.cmet.2012.12.012.

Fan W, Evans RM. 2017. Exercise Mimetics: Impact on Health and Performance. *Cell Metabolism* **25**:242–247. doi: 10.1016/j.cmet.2016.10.022.

Feige JN, Lagouge M, Canto C, Strehle A, Houten SM, Milne JC, Lambert PD, Mataki C, Elliott PJ, Auwerx J. 2008. Specific SIRT1 activation mimics low energy levels and protects against diet-induced metabolic disorders by enhancing fat oxidation. *Cell Metabolism* **8**:347–358. doi: 10.1016/j.cmet.2008.08.017.

Fernandes ES, Fernandes MA, Keeble JE. 2012. The functions of TRPA1 and TRPV1: moving away from sensory nerves. *British Journal of Pharmacology* **166**:510–521. doi: 10.1111/j.1476-5381.2012.01851.x.

Harb AA, Bustanji YK, Almasri IM, Abdalla SS. 2019. Eugenol Reduces LDL Cholesterol and Hepatic Steatosis in Hypercholesterolemic Rats by Modulating TRPV1 Receptor. *Scientific Reports* **9**:14003. doi: 10.1038/s41598-019-50352-4.

Hasan R, Zhang X. 2018. Ca2+ regulation of TRP ion channels. *International journal of molecular Sciences* **19**. doi: 10.3390/ijms19041256.

Hoehn KL, Turner N, Swarbrick MM, Wilks D, Preston E, Phua Y, Joshi H, Furler SM, Larance M, Hegarty BD, Leslie SJ, Pickford R, Hoy AJ, Kraegen EW, James DE, Cooney GJ. 2010. Acute or chronic upregulation of mitochondrial fatty acid oxidation has no net effect on whole-body energy expenditure or adiposity. *Cell Metabolism* **11**:70–76. doi: 10.1016/j.cmet.2009.11.008.

Hou N, He X, Yang Y, Fu J, Zhang W, Guo Z, Hu Y, Liang L, Xie W, Xiong H, Wang K, Pang M. 2019. TRPV1 induced apoptosis of colorectal cancer cells by activating calcineurin-NFAT2-p53 signaling pathway. *BioMed Research International* **2019**:6712536. doi: 10.1155/2019/6712536.

Jacquemin V, Butler-Browne GS, Furling D, Mouly V. 2007. IL-13 mediates the recruitment of reserve cells for fusion during IGF-1-induced hypertrophy of human myotubes. *Journal of Cell Science* **120**:670–681. doi: 10.1242/jcs.03371.

Jakobs C, Bartok E, Kubarenko A, Bauernfeind F, Hornung V. 2013. Immunoblotting for active caspase-1. *Methods in Molecular Biology* **1040**:103–115. doi: 10.1007/978-1-62703-523-1_9.

Jiang Y, Feng C, Shi Y, Kou X, Le G. 2022. Eugenol improves high-fat diet/streptomycin-induced type 2 diabetes mellitus (T2DM) mice muscle dysfunction by alleviating inflammation and increasing muscle glucose uptake. *Frontiers in Nutrition* **9**. doi: 10.3389/fnut.2022.1039753.

Jung CH, Ahn J, Jeon T-I, Kim TW, Ha TY. 2012. Syzygium aromaticum ethanol extract reduces high-fat diet-induced obesity in mice through downregulation of adipogenic and lipogenic gene expression. *Experimental and Therapeutic Medicine* **4**:409–414. doi: 10.3892/etm.2012.609.

Kaur G, Athar M, Alam MS. 2010. Eugenol precludes cutaneous chemical carcinogenesis in mouse by preventing oxidative stress and inflammation and by inducing apoptosis. *Molecular Carcinogenesis* **49**:290–301. doi: 10.1002/mc.20601.

Knudsen NH, Stanya KJ, Hyde AL, Chalom MM, Alexander RK, Liou Y-H, Starost KA, Gangl MR, Jacobi D, Liu S, Sopariwala DH, Fonseca-Pereira D, Li J, Hu FB, Garrett WS, Narkar VA, Ortlund EA, Kim JH, Paton CM, Cooper JA, Lee C-H. 2020. Interleukin-13 drives metabolic conditioning of muscle to endurance exercise. *Science* **368:**eaat3987. doi: 10.1126/science.aat3987.

Koplas PA, Rosenberg RL, Oxford GS. 1997. The role of calcium in the desensitization of capsaicin responses in rat dorsal root ganglion neurons. *The Journal of Neuroscience* **17**:3525–3537. doi: 10.1523/JNEUROSCI.17-10-03525.1997.

Lesgards J-F, Baldovini N, Vidal N, Pietri S. 2014. Anticancer activities of essential oils constituents and synergy with conventional therapies: a review. *Phytotherapy Research* **28**:1423–1446. doi: 10.1002/ptr.5165.

Luo Z, Ma L, Zhao Z, He H, Yang D, Feng X, Ma S, Chen X, Zhu T, Cao T, Liu D, Nilius B, Huang Y, Yan Z, Zhu Z. 2012. TRPV1 activation improves exercise endurance and energy metabolism through PGC-1α upregulation in mice. *Cell Research* **22**:551–564. doi: 10.1038/cr.2011.205.

Ma L, Zhong J, Zhao Z, Luo Z, Ma S, Sun J, He H, Zhu T, Liu D, Zhu Z, Tepel M. 2011. Activation of TRPV1 reduces vascular lipid accumulation and attenuates atherosclerosis. *Cardiovascular Research* **92**:504–513. doi: 10.1093/cvr/cvr245.

Magalhães CB, Casquilho NV, Machado MN, Riva DR, Travassos LH, Leal-Cardoso JH, Fortunato RS, Faffe DS, Zin WA. 2019. The anti-inflammatory and anti-oxidative actions of

eugenol improve lipopolysaccharide-induced lung injury. *Respiratory Physiology & Neurobiology* **259**:30–36. doi: 10.1016/j.resp.2018.07.001.

Men X-M, Xu Z-W, Tao X, Deng B, Qi K-K. 2021. FNDC5 expression closely correlates with muscle fiber types in porcine longissimus dorsi muscle and regulates myosin heavy chains (MyHCs) mRNA expression in C2C12 cells. *PeerJ* **9**:e11065. doi: 10.7717/peerj.11065.

Meng J, Lv Z, Sun C, Qiao X, Chen C. 2020. An extract of Lycium barbarum mimics exercise to improve muscle endurance through increasing type IIa oxidative muscle fibers by activating ERRγ. *FASEB Journal* **34**:11460–11473. doi: 10.1096/fj.202000136R.

Mnafgui K, Kaanich F, Derbali A, Hamden K, Derbali F, Slama S, Allouche N, Elfeki A. 2013. Inhibition of key enzymes related to diabetes and hypertension by Eugenol in vitro and in alloxan-induced diabetic rats. *Archives of Physiology and Biochemistry* **119**:225–233. doi: 10.3109/13813455.2013.822521.

Nadeau L, Aguer C. 2019. Interleukin-15 as a myokine: mechanistic insight into its effect on skeletal muscle metabolism. *Applied Physiology, Nutrition, and Metabolism* **44**:229–238. doi: 10.1139/apnm-2018-0022.

Narkar VA, Downes M, Yu RT, Embler E, Wang Y-X, Banayo E, Mihaylova MM, Nelson MC, Zou Y, Juguilon H, Kang H, Shaw RJ, Evans RM. 2008. AMPK and PPARδ agonists are exercise mimetics. *Cell* **134**:405–415. doi: 10.1016/j.cell.2008.06.051.

Nilius B, Owsianik G, Voets T, Peters JA. 2007. Transient receptor potential cation channels in disease. *Physiological Reviews* **87**:165–217. doi: 10.1152/physrev.00021.2006.

Nogueira L, Ramirez-Sanchez I, Perkins GA, Murphy A, Taub PR, Ceballos G, Villarreal FJ, Hogan MC, Malek MH. 2011. (-)-Epicatechin enhances fatigue resistance and oxidative

capacity in mouse muscle. *The Journal of Physiology* **589**:4615–4631. doi: 10.1113/jphysiol.2011.209924.

Pedersen BK, Febbraio MA. 2012. Muscles, exercise and obesity: skeletal muscle as a secretory organ. *Nature reviews. Endocrinology* **8**:457–465. doi: 10.1038/nrendo.2012.49.

Quinn LS, Anderson BG, Conner JD, Wolden-Hanson T. 2013. IL-15 overexpression promotes endurance, oxidative energy metabolism, and muscle PPARδ, SIRT1, PGC-1α, and PGC-1β expression in male mice. *Endocrinology* **154**:232–245. doi: 10.1210/en.2012-1773.

Rangwala SM, Wang X, Calvo JA, Lindsley L, Zhang Y, Deyneko G, Beaulieu V, Gao J, Turner G, Markovits J. 2010. Estrogen-related receptor gamma is a key regulator of muscle mitochondrial activity and oxidative capacity. *The Journal of Biological Chemistry* **285**:22619–22629. doi: 10.1074/jbc.M110.125401.

Rodrigues M, Bertoncini-Silva C, Joaquim AG, Machado CD, Ramalho LNZ, Carlos D, Fassini PG, Suen VMM. 2022. Beneficial effects of eugenol supplementation on gut microbiota and hepatic steatosis in high-fat-fed mice. *Food & Function* **13**:3381–3390. doi: 10.1039/d1fo03619j.

Sakuma K, Yamaguchi A. 2010. The functional role of calcineurin in hypertrophy, regeneration, and disorders of skeletal muscle. *Journal of Biomedicine & Biotechnology* **2010**:721219. doi: 10.1155/2010/721219.

Sanae F, Kamiyama O, Ikeda-Obatake K, Higashi Y, Asano N, Adachi I, Kato A. 2014. Effects of eugenol-reduced clove extract on glycogen phosphorylase b and the development of diabetes in db/db mice. *Food & Function* **5**:214–219. doi: 10.1039/c3fo60514k.

Sanz-Salvador L, Andrés-Borderia A, Ferrer-Montiel A, Planells-Cases R. 2012. Agonist- and Ca2+-dependent desensitization of TRPV1 channel targets the receptor to lysosomes for

degradation. *The Journal of Biological Chemistry* **287**:19462–19471. doi: 10.1074/jbc.M111.289751.

Schiaffino S, Reggiani C. 2011. Fiber types in mammalian skeletal muscles. *Physiological Reviews* **91**:1447–1531. doi: 10.1152/physrev.00031.2010.

Severinsen MCK, Pedersen BK. 2020. Muscle-organ crosstalk: The emerging roles of myokines. *Endocrine Reviews* **41**. doi: 10.1210/endrev/bnaa016.

Srinivasan S, Sathish G, Jayanthi M, Muthukumaran J, Muruganathan U, Ramachandran V. 2014. Ameliorating effect of eugenol on hyperglycemia by attenuating the key enzymes of glucose metabolism in streptozotocin-induced diabetic rats. *Molecular and Cellular Biochemistry* **385**:159–168. doi: 10.1007/s11010-013-1824-2.

Wang P, Yan Z, Zhong J, Chen J, Ni Y, Li L, Ma L, Zhao Z, Liu D, Zhu Z. 2012. Transient receptor potential vanilloid 1 activation enhances gut glucagon-like peptide-1 secretion and improves glucose homeostasis. *Diabetes* **61**:2155–2165. doi: 10.2337/db11-1503.

Welinder C, Ekblad L. 2011. Coomassie staining as loading control in Western blot analysis. *Journal of Proteome Research* **10**:1416–1419. doi: 10.1021/pr1011476.

Wen W, Chen X, Huang Z, Chen D, Chen H, Luo Y, He J, Zheng P, Yu J, Yu B. 2020. Resveratrol regulates muscle fiber type conversion via miR-22-3p and AMPK/SIRT1/PGC-1α pathway. *The Journal of Nutritional Biochemistry* **77**:108297. doi: 10.1016/j.jnutbio.2019.108297.

Whitham M, Febbraio MA. 2016. The ever-expanding myokinome: discovery challenges and therapeutic implications. *Nature Reviews. Drug Discovery* **15**:719–729. doi: 10.1038/nrd.2016.153.

Xu H, Delling M, Jun JC, Clapham DE. 2006. Oregano, thyme and clove-derived flavors and skin sensitizers activate specific TRP channels. *Nature Neuroscience* **9**:628–635. doi: 10.1038/nn1692.

Yang BH, Piao ZG, Kim Y-B, Lee C-H, Lee JK, Park K, Kim JS, Oh SB. 2003. Activation of vanilloid receptor 1 (VR1) by eugenol. *Journal of Dental Research* **82**:781–785. doi: 10.1177/154405910308201004.

Yang J, Rothermel B, Vega RB, Frey N, McKinsey TA, Olson EN, Bassel-Duby R, Williams RS. 2000. Independent signals control expression of the calcineurin inhibitory proteins MCIP1 and MCIP2 in striated muscles. *Circulation Research* **87**:E61-E68. doi: 10.1161/01.res.87.12.e61.

Yang Y, Guo W, Ma J, Xu P, Zhang W, Guo S, Liu L, Ma J, Shi Q, Jian Z, Liu L, Wang G, Gao T, Han Z, Li C. 2018. Downregulated TRPV1 expression contributes to melanoma growth via the calcineurin-ATF3-p53 pathway. *The Journal of Investigative Dermatology* **138**:2205–2215. doi: 10.1016/j.jid.2018.03.1510.

Zádor E. 2008. dnRas stimulates autocrine-paracrine growth of regenerating muscle via calcineurin-NFAT-IL-4 pathway. *Biochemical and Biophysical Research Communications* **375**:265–270. doi: 10.1016/j.bbrc.2008.08.024.

Figures and Tables

Table 1 Myokines to be tested in our study.

	Myokines	References
Myokines that improve metabolic homeostasis	CX3CL1, FGF21, FNDC5, IL-6, IL-8, IL-15	***(Whitham, M., and Febbraio, M.A, 2016)***
	Metrnl, FGF21, FNDC5, Myonectin	(***Eckel, 2019***)
Myokines that improve endurace capacity and promote fast to slow muscle fiber transformation	FNDC5	***(Men et al., 2021)***
	IL-13	(***Knudsen et al., 2020***)
	IL-15	(***Quinn et al., 2013***)
	Neurturin	(***Correia et al., 2021***)

732 **Figure captions**

733 **Figure 1. Eugenol promotes the transformation of fast to slow musle fiber. (A)** The body
734 weight of the mice. (**B, C**), Skeletal muscle weight and representative images of skeletal muscle.
735 **(D-F)** The protein expression of muscle fiber type in GAS and TA muscle and in C2C12
736 myotubes. (**G-H)** The mRNA expression of muscle fiber type in GAS and TA muscle and in
737 C2C12 myotubes. For A-B, N=12 per group. For D-E, N=3 per group. For F and H, N=4 per
738 group. For G, N=6 per group. *$P < 0.05$, **$P < 0.01$, and ***$P < 0.001$.

739 **Figure 1-figure supplement 1. Effect of eugenol on C2C12 cell viability.** Cells were treated
740 with 0, 12.5, 25, 50, 100, 200 μM EUG for 1 day after 4 days of differentiation. The C2C12 cell
741 viability was measured using CCK-8 kit. N=6 per group. *P < 0.05, **P < 0.01, and ***P <
742 0.001.

743 **Figure 2. Eugenol promotes oxidative metabolism activity, mitochondrial function, and**
744 **endurance performance of mice. (A)** The effect of eugenol on exhausting swimming time in
745 mice. **(B)** The effect of eugenol on metabolism enzymes activity in GAS and TA muscle. (**C)** The
746 heatmap for the mRNA expression of genes encoding mitochondrial complex components and
747 transcription factors controling mitochondrial biogenesis in GAS muscle. Color gradient
748 represents relative mRNA expression with darker colors indicating higher expression. **(D)** Protein
749 expression of mitochondrial electron transport complexes in GAS muscle. Complex I (NDUFA1),
750 complex II (SDHA), complex III (UQCRC1), complex IV (MTCO1), and comlex V (ATP5B). (**E)**
751 mtDNA copy number in muscles and cells. For A, N=15 per group. For B, N=6 per group. For C
752 and F, N=4 per group. For D, N=3 per group. For E, N=6 per group. $^{\#}P<0.1$, *$P < 0.05$, **$P <$
753 0.01, and ***$P < 0.001$.

754 **Figure 3. Eugenol enhances lipolysis and thermogenesis.** (**A)** The ADF and the ration of ADF
755 to ADG. (**B)** Tissue weight of adipose weight. (**C)** The level of T-CHO, LDL, and HDL in serum.
756 (**D)** The mRNA expression of genes related to lipolysis, lipogenesis, and lipid transport in iWAT

757 and gWAT. (**E)** The mRNA expression of genes related to adipose browning and thermogenesis in
758 iWAT and gWAT. (**F)** The protein expression of FABP1 and UCP1 in iWAT and gWAT. (**G)** The
759 expression of protein related to adipose browning and thermogenesis in BAT. (**H)** The protein
760 expression of mitochondrial electron transport complexes in BAT. For A-B, N=12 per group. For
761 C-E, N=6 per group. For F-H, N=3 per group. $^{\#}P<0.1$, $^{*}P < 0.05$, $^{**}P < 0.01$, and $^{***}P < 0.001$.

762 **Figure 4. Eugenol activated TRPV1-mediated CaN/NFATc1 signaling pathway.** (**A)** The gene
763 expression profile of TRP channels in skeletal muscle was obtained from the GTEx dataset in The
764 Human Protein Atlas (https://www.proteinatlas.org/). (**B, C)** The mRNA expression of TRP
765 channels in TA muscle and C2C12 myotubes. (**D-F)** The TRPV1 and CnA protein expression in
766 GAS and TA muscle and in C2C12 myotubes. (**G-I)** The protein expression of NFATc1 in GAS
767 and TA muscle and in C2C12 myotubes. For B, N=6 per group. For C, F, and I, N=4 per group.
768 For D-E and G-H, N=3 per group. $^{*}P < 0.05$, $^{**}P < 0.01$, and $^{***}P < 0.001$.

769 **Figure 4-figure supplement 1. TRP channels expression profiles and *TRPV1* mRNA**
770 **eexpression in adipose tissue.** The gene expression profile was obtained from the GTEx dataset
771 in The Human Protein Atlas (https://www.proteinatlas.org/). (**A)** TRPV1 expression profiles in
772 tissues. (**B)** TRP channels expression profiles in adipose tissue. (**C)** The mRNA expression of
773 TRP channels in adipose tissue. For C, N=6 per group. $^{\#}P<0.1$, $^{*}P < 0.05$, $^{**}P < 0.01$, and $^{***}P <$
774 0.001.

775 **Figure 4-figure supplement 2. Molecular docking for eugenol and TRPV1.** The capsaicin
776 binding sites (TYR511, SER512, THR550, and GLU570) were selected as the binding pocket.
777 The figure showed TRPV1 amino acid residues interacting with eugenol and the intermolecular
778 force.

779 **Figure 4-figure supplement 3. The mRNA expression of *MCIP1*.** N=6 per group. $^{*}P < 0.05$,
780 $^{**}P < 0.01$, and $^{***}P < 0.001$.

781 **Figure 5. Eugenol promotes fast to slow muscle fiber transformation by activating TRPV1-**
782 **mediated CaN/NFATc1 signaling pathway.** C2C12 myotubes were treated by 25 μM eugenol
783 and 1 μM TRPV1 inhibitor AMG-517 or 0.5 μM CaN inhibitor CsA for 1 day after 4 days of
784 differentiation. (**A**) The flow cytometry assay was used to detect Ca^{2+} levels in C2C12 myotubes;
785 FITC means the fluo-4 fluorescence and SSC means side scatter. **(B)** Western blot was uesd to
786 detect CnA protein expression in C2C12 myotubes. **(C)** Western blot was uesd to detect
787 mitochondrial electron transport complexes protein expression in C2C12 myotubes. (**D**) Western
788 blot was uesd to detect slow MyHC and fast MyHC protein expression in C2C12 myotubes. (**E**)
789 Representative immunofluorescence images of Slow MyHC (Green fluorescence) and relative
790 mean fluorescence intensity quantification. Magnification: × 200. For A-D, N=4 per group. $*P <$
791 0.05, $**P < 0.01$, and $***P < 0.001$.

792 **Figure 6. The myokines controlled by CaN.** C2C12 myotubes were treated for 16 h with 0, 0.1,
793 0.5, and 1 μM Ca^{2+} ionophore after 2 days of differentiation. (**A**) The mRNA expression of
794 *MCIP1*. (**B**) The protein expression of CnA. (**C**) The enzyme activity of CaN. (**D**) Fluo-4 was
795 used to stain the Ca^{2+} and the flow cytometry assay was used to detect Ca^{2+} fluorescence in
796 C2C12 myotubes in control and 0.5 μM A23187 groups. (**E**) The heatmap for the myokines
797 mRNA expression in control and 0.5 μM A23187 groups. Color gradient represents relative
798 mRNA expression with darker colors indicating higher expression. **(F)** Correlation analysis of
799 gene expression values of myokines and MCIP1 gene performed by linear regression with
800 Pearson's correlation coefficient (r). Color gradient represents correlation coefficient with darker
801 colors indicating higher positive correlation. (**G**) The number of binding sites for transcription
802 factors NFATc1 were predicted by hTFtarget and JASPAR. For A, N=6 per group. For B-D, N=3
803 per group. For E, N=4 per group. $*P < 0.05$, $**P < 0.01$, and $***P < 0.001$.

804 **Figure 7. The myokine IL-15 expression depends on CaN/NFATc1 signaling pathway. (A)**
805 C2C12 myotubes were treated for 16 h with 0, 0.1, 0.5, and 1 μM Ca^{2+} ionophore after 2 days of

differentiation. The protein expression of IL-15. (**B-D)** C2C12 myotubes were treated by 0.5 μM A23187 and 0.5 μM CsA for 16 h after 2 days of differentiation. The protein expression of CnA, NFATc1, and IL-15. **(E)** Sequence logo of NFATc1 motif and the predicted NFATc1 binding sites in the promoter region of IL-15. **(F)** NFATc1 and the key sequence of IL-15 (5'-AATGAAAA-3') docking. Confidence scores above 0.7 indicate high probability of binding, scores between 0.5 and 0.7 suggest possible binding, and scores below 0.5 indicate unlikely binding. (**G)** The probe sequence of NFATc1. The underline represents the predicted binding site of NFATc1, bio-NFATc1 means oligonucleotide probes that labeled with biotin at the 5' end, cold-NFATc1 means oligonucleotide probes that did not labeled with biotin, mu-NFATc1 means oligonucleotide probes that was mutated at the binding site. (**H)** Nuclear protein extracts (NE) with NFATc1 probe were used to EMSA assay. (**I)** The protein expression of NFATc1 after transfecting 1 μg/mL pcDNA3.1 vector, 0.5 μg/mL or 1 μg/mL pcDNA3.1-NFATc1 in HEK293T cells. (**J)** The relative luciferase intensity referred to the ratio between firefly luciferase intensity and renilla luciferase intensity. For A-D, N=3 per group. For H, N=6 per group. *P < 0.05, **P < 0.01, and ***P < 0.001.

Figure 7-figure supplement 1. Ca^{2+} ionophore A23187 promotes the transformation of fast to slow muscle fiber by CaN signaling pathway. A-C The mRNA and protein expression of muscle fiber type in C2C12 myotubes. For B, N=4 per group. For A and C, N=3 per group. *P < 0.05, **P < 0.01, and ***P < 0.001.

824 **Figure 8. Eugenol promotes the expression and secretion of IL-15 in skeletal muscle of mice.**
825 (**A)** The *IL-15* mRNA expression in GAS and TA muscle. **(B, C)** The IL-15 protein expression in
826 GAS and TA muscle. (**D)** Left: The mRNA expression of *MyHC I*, *MyHC IIa*, *MyHC IIb* and *IL-*
827 *15* in EDL and SOL muscle of mice. Right: Correlation analysis of gene expression values
828 performed by linear regression with Pearson's correlation coefficient (r). Color gradient represents
829 correlation coefficient with darker colors indicating higher positive correlation. (**E)** The protein
830 expreesion of slow MyHC, fast MyHC, and IL-15. (**F)** The concertration of IL-15 in serum. For
831 A, D, and F, N=6 per group. For B-C and E, N=3 per group. *$P < 0.05$, **$P < 0.01$, and ***$P <$
832 0.001.

833 **Figure 9. Eugenol promotes IL-15 level through TRPV1-mediated CaN/NFATc1 signaling**
834 **pathway.** C2C12 myotubes were treated by 0-200 eugenol for 1 day after 4 days of
835 differentiation. (**A)** The effect of eugenol on *IL-15* mRNA expression in C2C12 myotubes. (**B)**
836 The effect of eugenol on IL-15 protein expression in the C2C12 cell medium. Coomassie staining
837 as loading control. **(C, D)** C2C12 myotubes were treated by 25 μM eugenol and 1 μM TRPV1
838 inhibitor AMG-517 or 0.5 μM CaN inhibitor CsA for 1 day after 4 days of differentiation. The
839 mRNA and protein expression of IL-15. N=4 per group. *$P < 0.05$, **$P < 0.01$, and ***$P < 0.001$.

840 **Figure 9-figure supplement 1. Representative immunofluorescence images of IL-15.** IL-15
841 (Green fluorescence) and DAPI (Blue fluorescence). Magnification: × 200.

842

Source data files

Figure 1-Source Data 1. Western blot raw image.

Figure 2-Source Data 1. Western blot raw image.

Figure 3-Source Data 1. Western blot raw image.

Figure 4-Source Data 1. Western blot raw image.

Figure 5-Source Data 1. Western blot raw image.

Figure 6-Source Data 1. Western blot raw image.

Figure 7-Source Data 1. Western blot raw image.

Figure 8-Source Data 1. Western blot raw image.

Figure 9-Source Data 1. Western blot raw image.

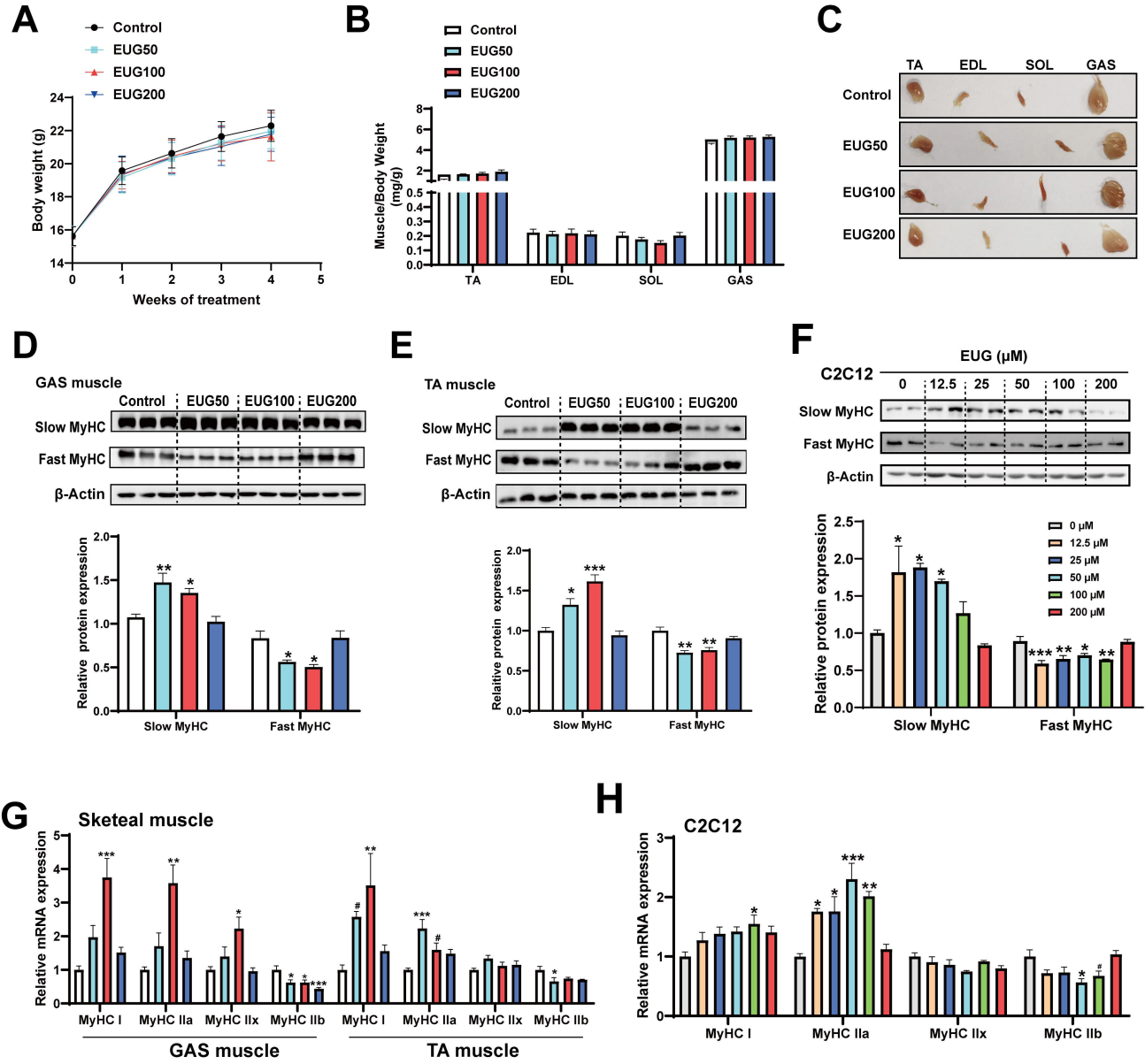
A
Control
EUG50
EUG100
EUG200
Body weight (g)
Weeks of treatment
B
Control
EUG50
EUG100
EUG200
Muscle/Body Weight (mg/g)
TA
EDL
SOL
GAS
C
TA
EDL
SOL
GAS
Control
EUG50
EUG100
EUG200
D
GAS muscle
Control
EUG50
EUG100
EUG200
Slow MyHC
Fast MyHC
β-Actin
Relative protein expression
Slow MyHC
Fast MyHC
E
TA muscle
Control
EUG50
EUG100
EUG200
Slow MyHC
Fast MyHC
β-Actin
Relative protein expression
Slow MyHC
Fast MyHC
F
C2C12
EUG (μM)
0
12.5
25
50
100
200
Slow MyHC
Fast MyHC
β-Actin
Relative protein expression
0 μM
12.5 μM
25 μM
50 μM
100 μM
200 μM
Slow MyHC
Fast MyHC
G
Sketeal muscle
Relative mRNA expression
MyHC I
MyHC IIa
MyHC IIx
MyHC IIb
MyHC I
MyHC IIa
MyHC IIx
MyHC IIb
GAS muscle
TA muscle
H
C2C12
Relative mRNA expression
MyHC I
MyHC IIa
MyHC IIx
MyHC IIb

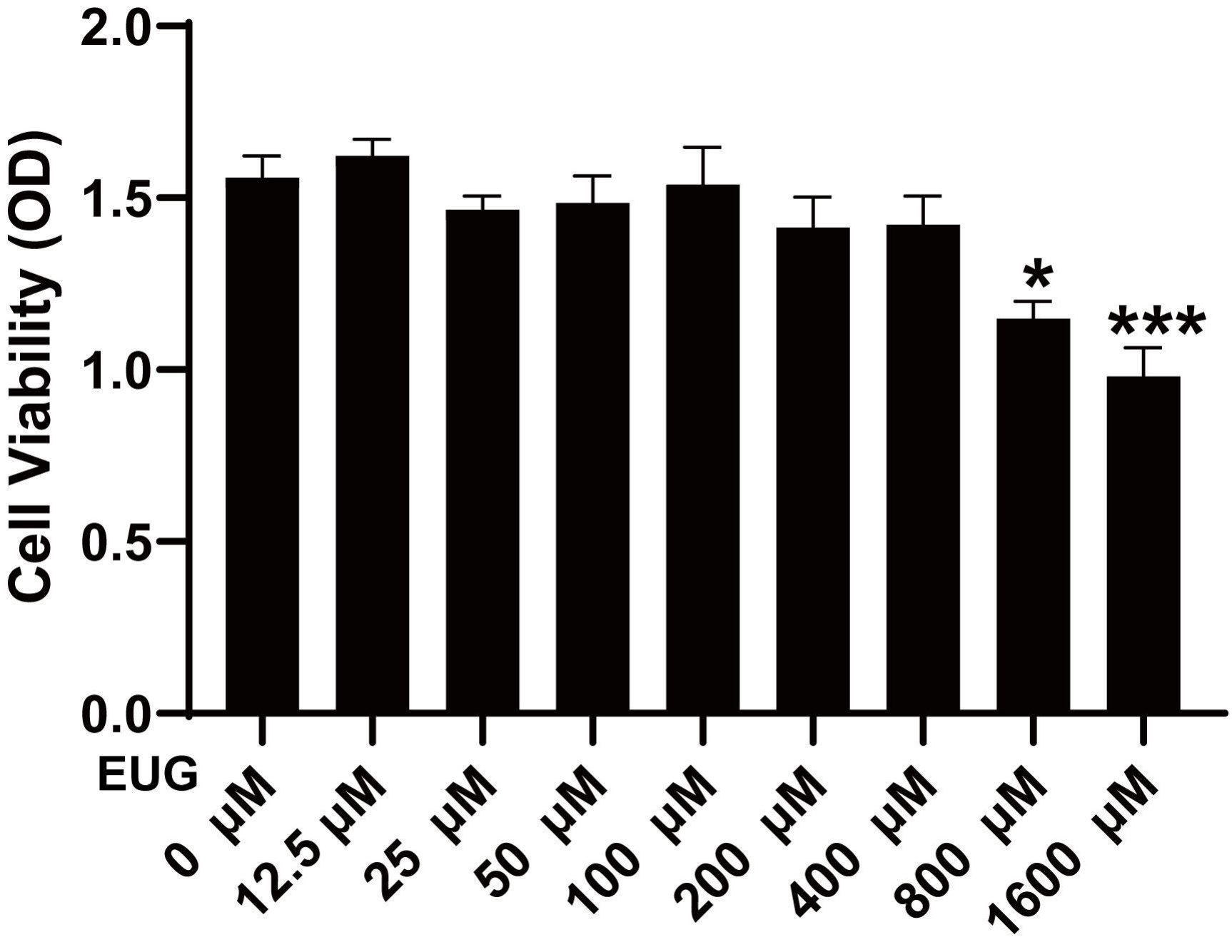
Cell Viability (OD)
2.0
1.5
1.0
0.5
0.0
*
***
EUG
0 μM
12.5 μM
25 μM
50 μM
100 μM
200 μM
400 μM
800 μM
1600 μM

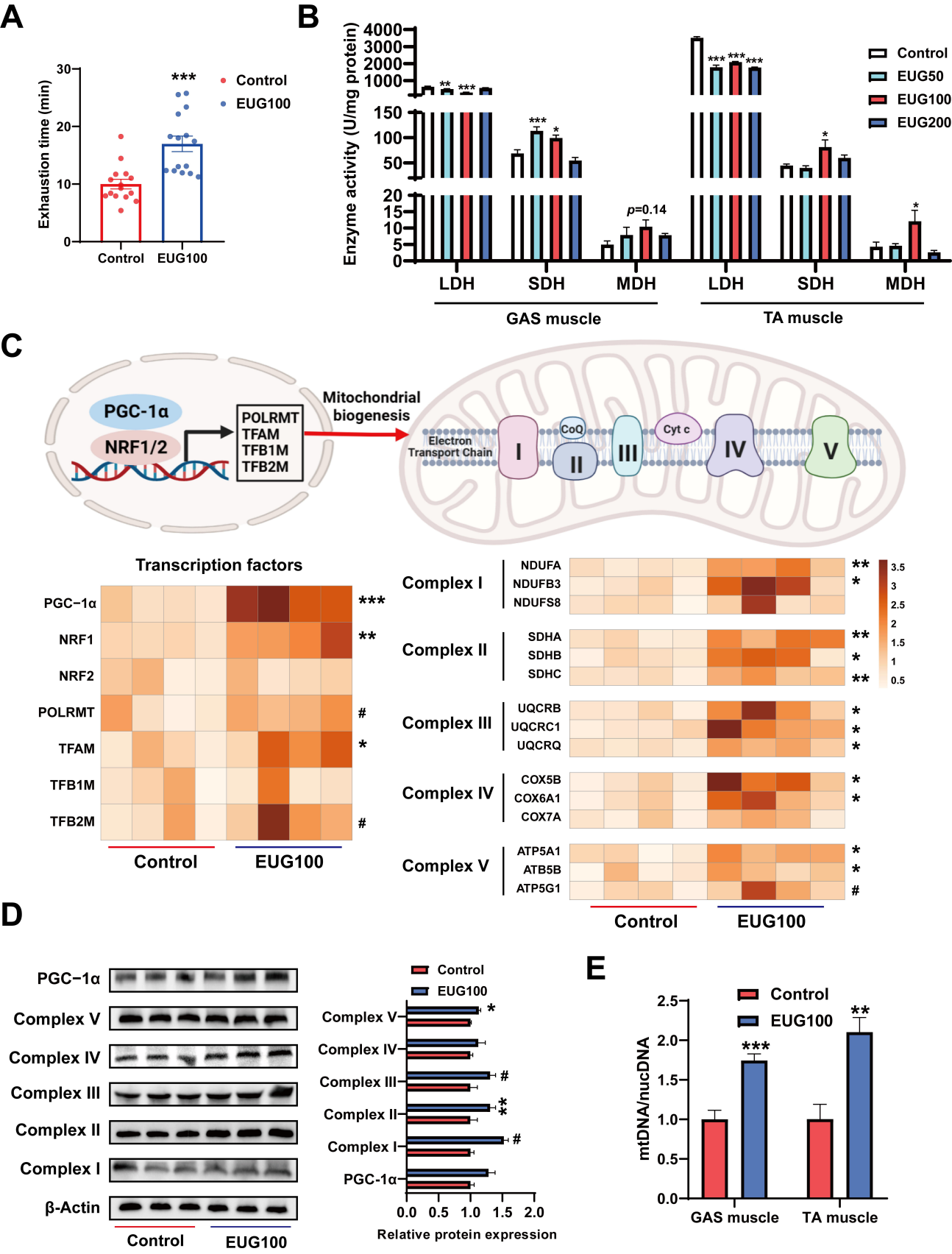
A
Exhaustion time (min)
Control
EUG100
B
Enzyme activity (U/mg protein)
Control
EUG50
EUG100
EUG200
p=0.14
LDH
SDH
MDH
GAS muscle
TA muscle
C
PGC-1α
NRF1/2
POLRMT
TFAM
TFB1M
TFB2M
Mitochondrial biogenesis
Electron Transport Chain
CoQ
Cyt c
Transcription factors
PGC-1α
NRF1
NRF2
POLRMT
TFAM
TFB1M
TFB2M
Complex I
NDUFA
NDUFB3
NDUFS8
Complex II
SDHA
SDHB
SDHC
Complex III
UQCRB
UQCRC1
UQCRQ
Complex IV
COX5B
COX6A1
COX7A
Complex V
ATP5A1
ATB5B
ATP5G1
D
PGC-1α
Complex V
Complex IV
Complex III
Complex II
Complex I
β-Actin
Relative protein expression
E
mtDNA/nucDNA
GAS muscle
TA muscle

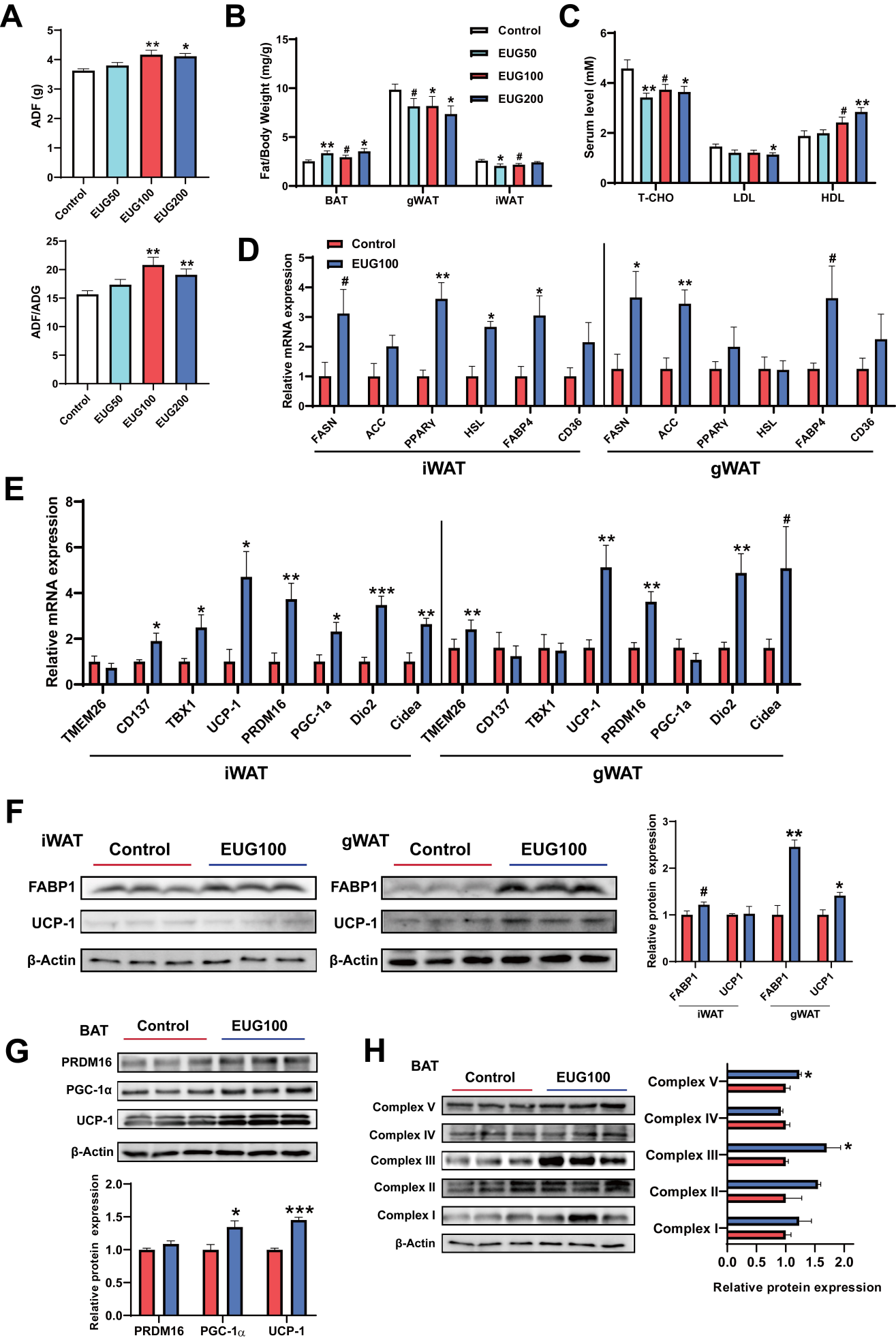
A
ADF (g)
Control
EUG50
EUG100
EUG200
ADF/ADG
B
Fat/Body Weight (mg/g)
BAT
gWAT
iWAT
C
Serum level (mM)
T-CHO
LDL
HDL
D
Relative mRNA expression
FASN
ACC
PPARγ
HSL
FABP4
CD36
iWAT
gWAT
E
Relative mRNA expression
TMEM26
CD137
TBX1
UCP-1
PRDM16
PGC-1a
Dio2
Cidea
iWAT
gWAT
F
iWAT
Control
EUG100
FABP1
UCP-1
β-Actin
gWAT
Relative protein expression
G
BAT
PRDM16
PGC-1α
UCP-1
β-Actin
Relative protein expression
H
BAT
Complex V
Complex IV
Complex III
Complex II
Complex I
β-Actin
Relative protein expression

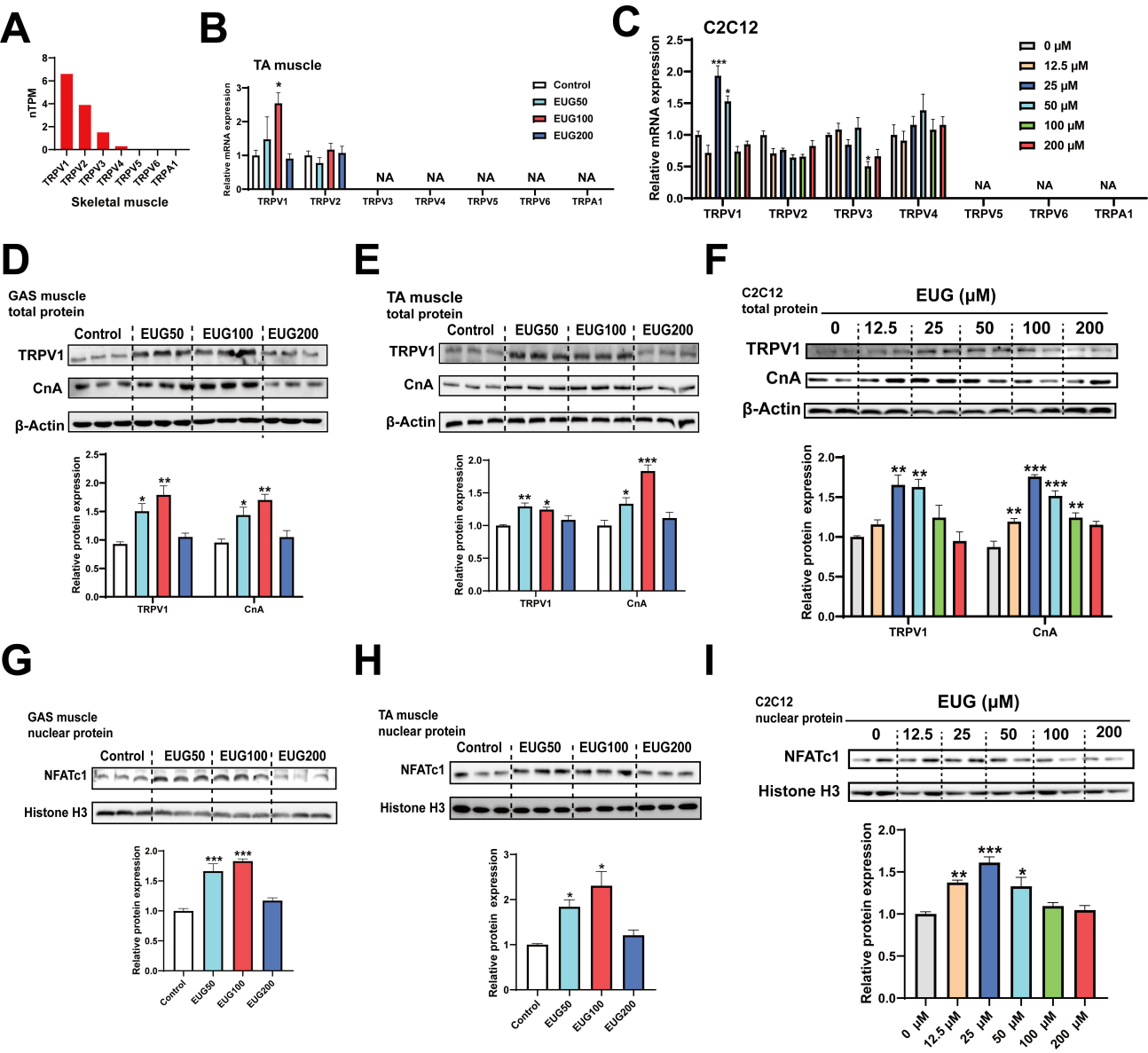
A
nTPM
Skeletal muscle
TRPV1
TRPV2
TRPV3
TRPV4
TRPV5
TRPV6
TRPA1
B
TA muscle
Relative mRNA expression
Control
EUG50
EUG100
EUG200
NA
C
C2C12
Relative mRNA expression
0 μM
12.5 μM
25 μM
50 μM
100 μM
200 μM
D
GAS muscle
total protein
Control
EUG50
EUG100
EUG200
TRPV1
CnA
β-Actin
Relative protein expression
E
TA muscle
total protein
F
C2C12
total protein
EUG (μM)
0
12.5
25
50
100
200
G
GAS muscle
nuclear protein
NFATc1
Histone H3
H
TA muscle
nuclear protein
I
C2C12
nuclear protein

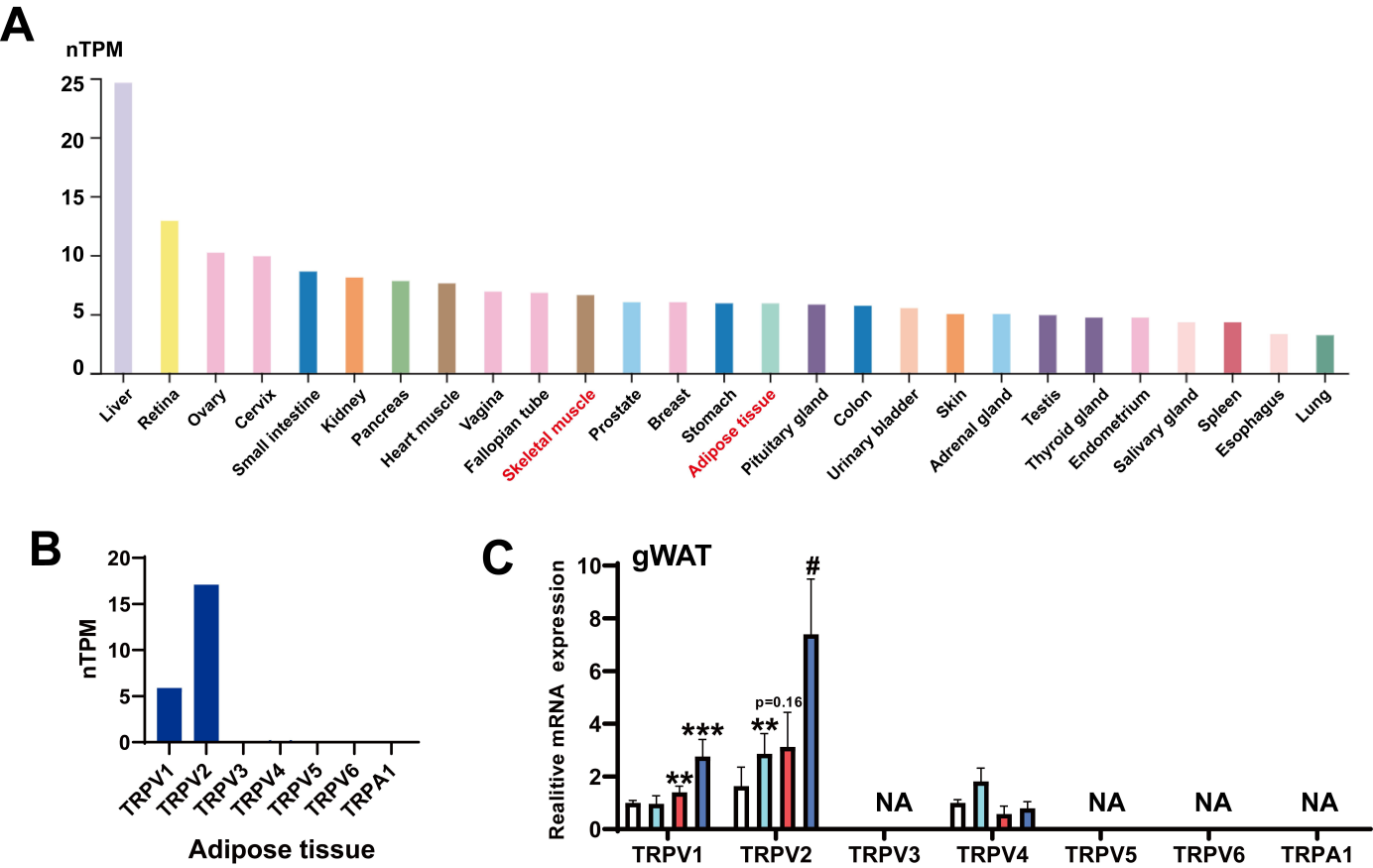
A
nTPM
25
20
15
10
5
0
Liver
Retina
Ovary
Cervix
Small intestine
Kidney
Pancreas
Heart muscle
Vagina
Fallopian tube
Skeletal muscle
Prostate
Breast
Stomach
Adipose tissue
Pituitary gland
Colon
Urinary bladder
Skin
Adrenal gland
Testis
Thyroid gland
Endometrium
Salivary gland
Spleen
Esophagus
Lung
B
nTPM
20
15
10
5
0
TRPV1
TRPV2
TRPV3
TRPV4
TRPV5
TRPV6
TRPA1
Adipose tissue
C
gWAT
Realitive mRNA expression
10
8
6
4
2
0
#
p=0.16
**
***
**
NA
NA
NA
NA
TRPV1
TRPV2
TRPV3
TRPV4
TRPV5
TRPV6
TRPA1

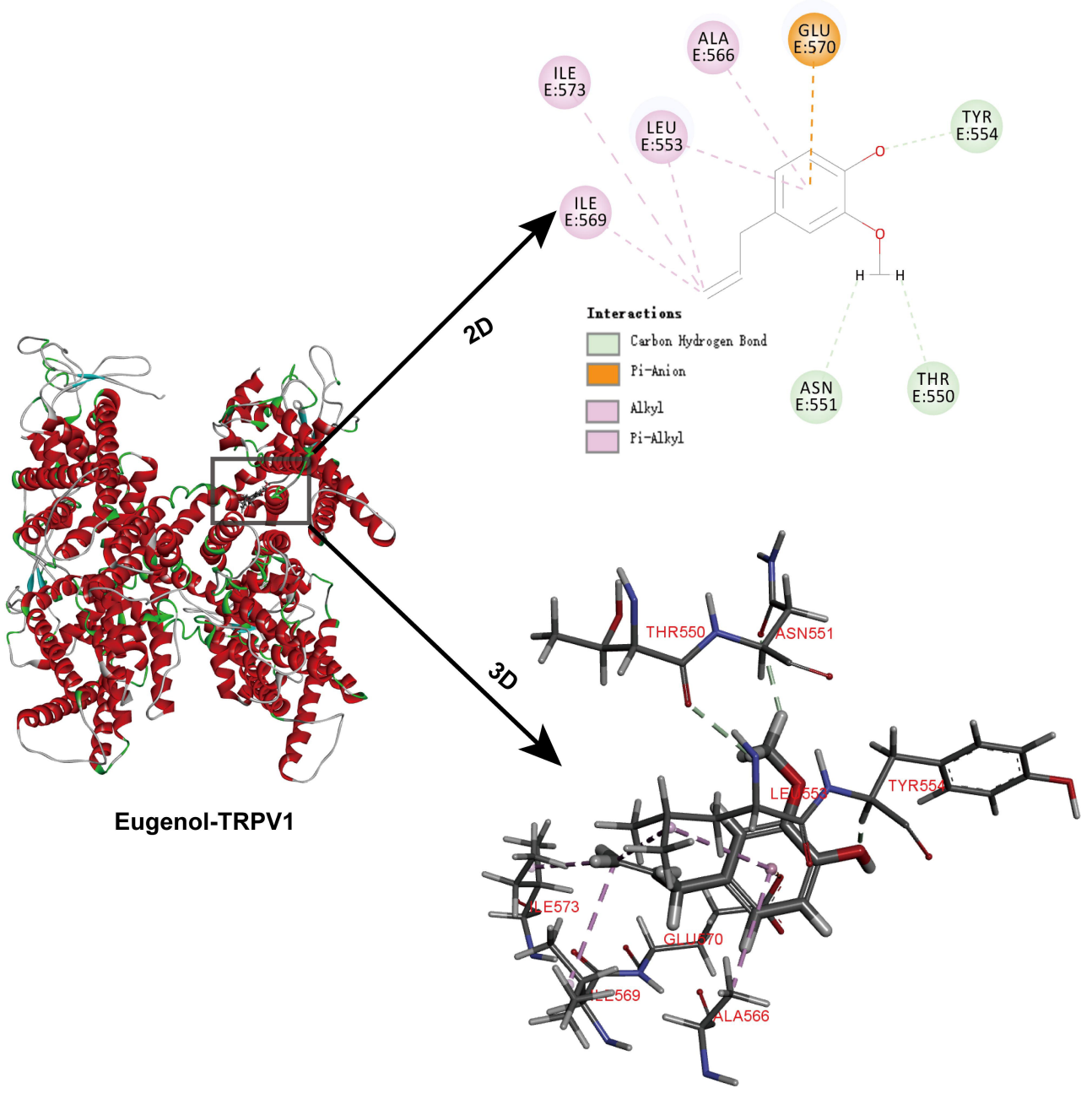
ILE E:573
ALA E:566
GLU E:570
LEU E:553
TYR E:554
ILE E:569
O
O
H
H
Interactions
Carbon Hydrogen Bond
Pi-Anion
Alkyl
Pi-Alkyl
ASN E:551
THR E:550
2D
3D
THR550
ASN551
TYR554
ILE573
ILE569
ALA566
Eugenol-TRPV1

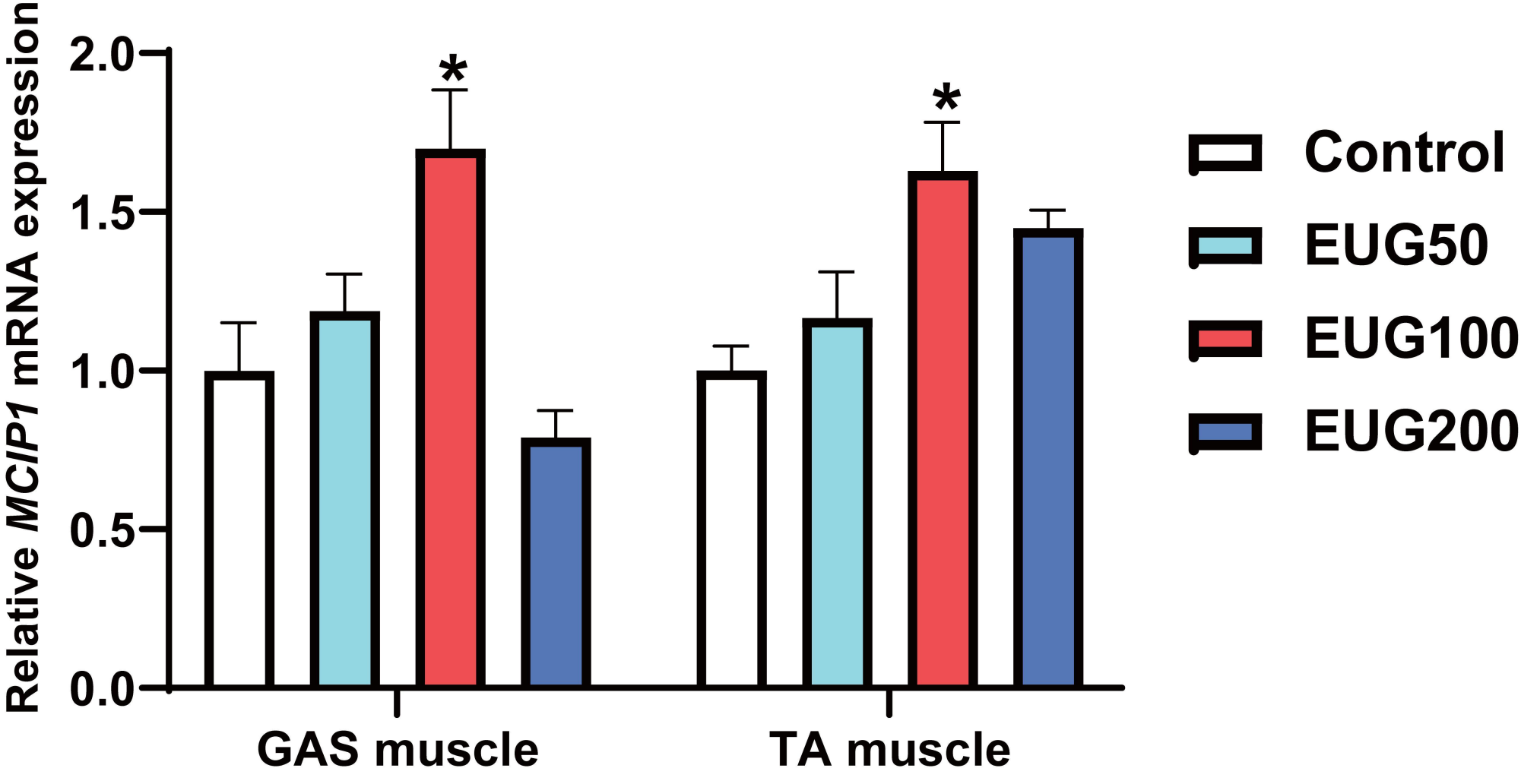
Relative MCIP1 mRNA expression
2.0
1.5
1.0
0.5
0.0
*
*
GAS muscle
TA muscle
Control
EUG50
EUG100
EUG200

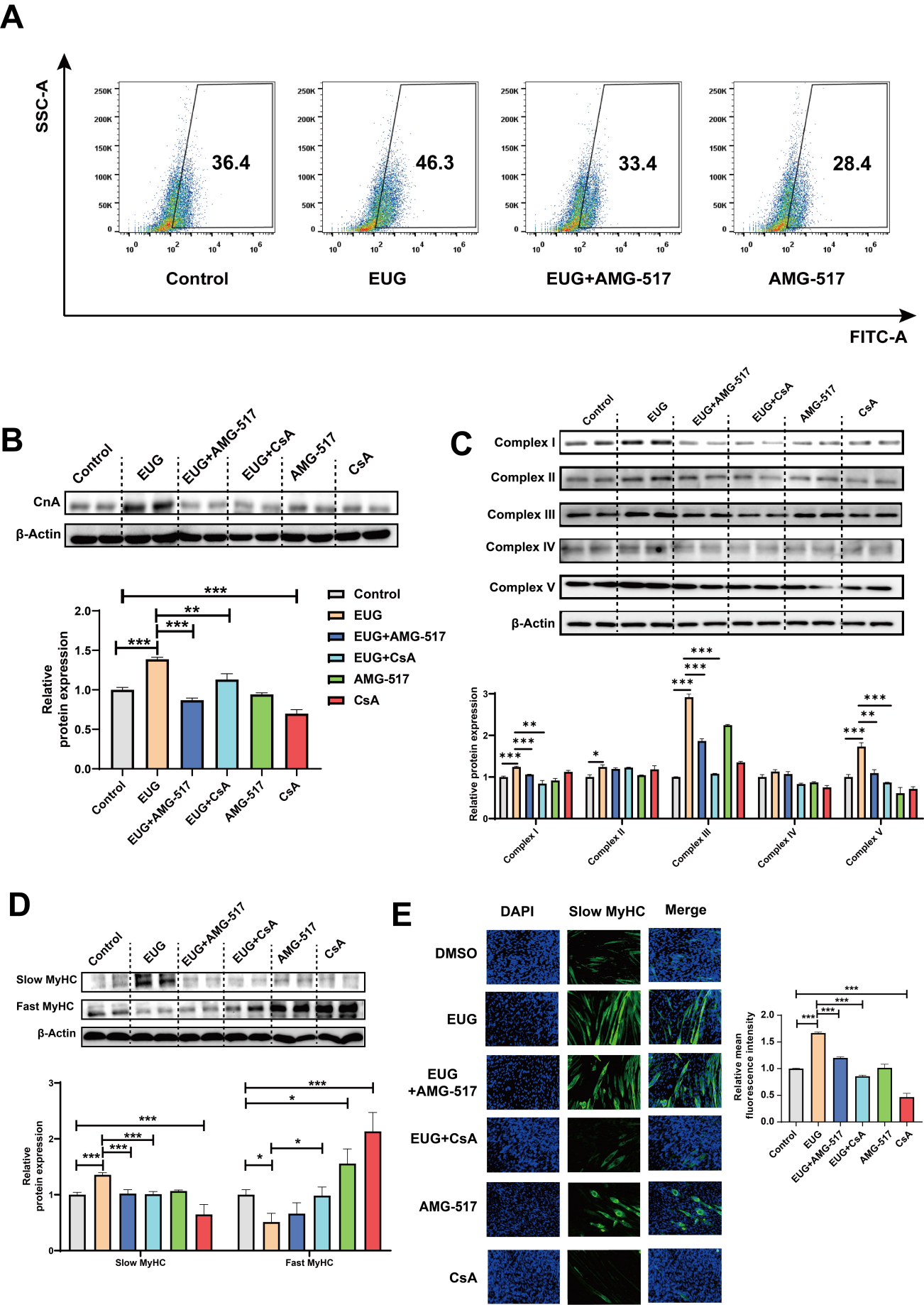
A
SSC-A
FITC-A
36.4
46.3
33.4
28.4
Control
EUG
EUG+AMG-517
AMG-517
B
Control
EUG
EUG+AMG-517
EUG+CsA
AMG-517
CsA
CnA
β-Actin
Relative protein expression
C
Complex I
Complex II
Complex III
Complex IV
Complex V
β-Actin
D
Slow MyHC
Fast MyHC
β-Actin
E
DAPI
Slow MyHC
Merge
DMSO
EUG
EUG +AMG-517
EUG+CsA
AMG-517
CsA
Relative mean fluorescence intensity

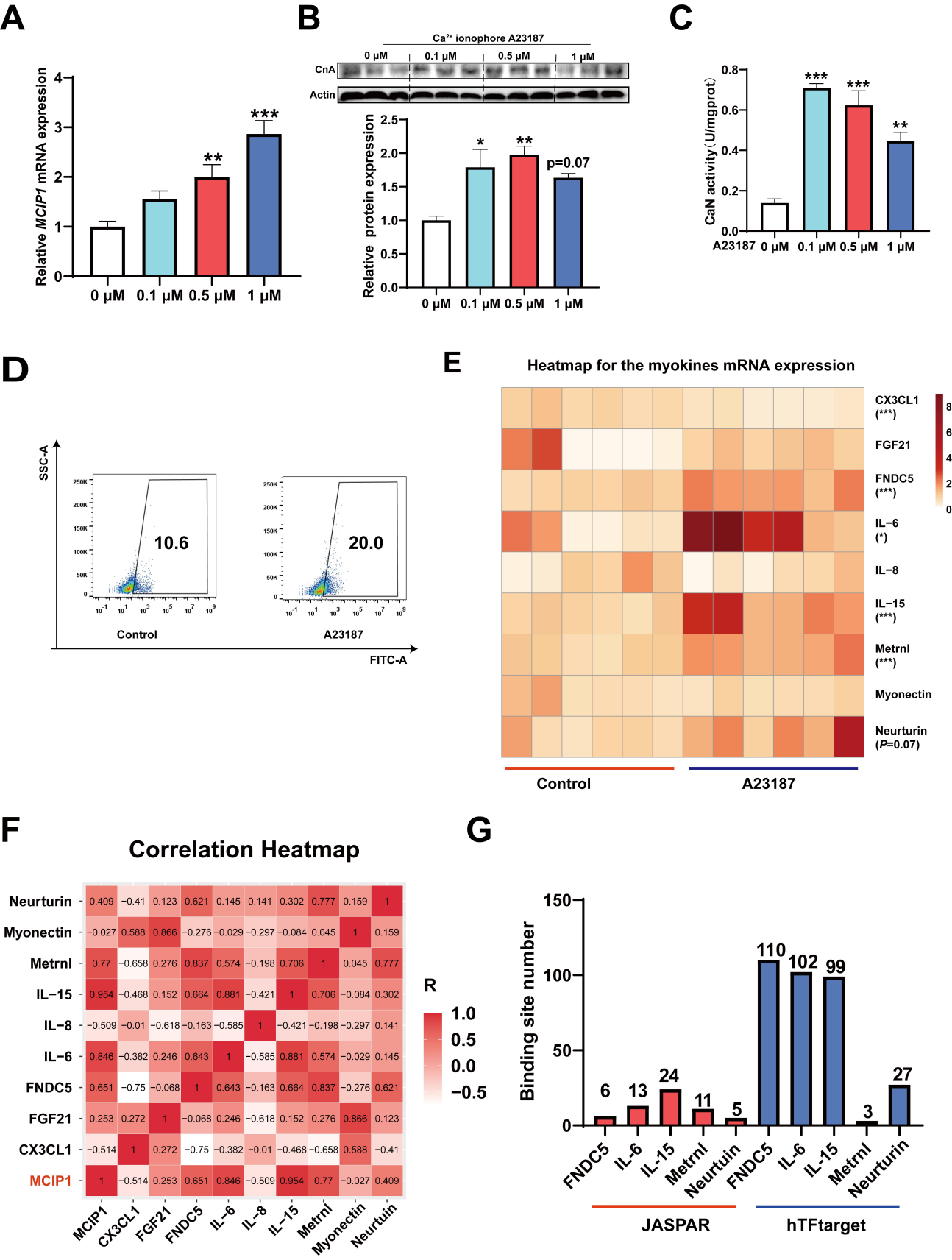
A
Relative MCIP1 mRNA expression
0 μM
0.1 μM
0.5 μM
1 μM
B
Ca²⁺ ionophore A23187
CnA
Actin
Relative protein expression
p=0.07
C
CaN activity (U/mgprot)
A23187
D
SSC-A
FITC-A
Control
A23187
10.6
20.0
E
Heatmap for the myokines mRNA expression
CX3CL1 (***)
FGF21
FNDC5 (***)
IL−6 (*)
IL−8
IL−15 (***)
MetrnI (***)
Myonectin
Neurturin (P=0.07)
Control
A23187
F
Correlation Heatmap
R
MCIP1
CX3CL1
FGF21
FNDC5
IL−6
IL−8
IL−15
MetrnI
Myonectin
Neurtuin
G
Binding site number
FNDC5
IL-6
IL-15
MetrnI
Neurtuin
JASPAR
hTFtarget

A
Ca2+ ionophore A23187
0 μM
0.1 μM
0.5 μM
1 μM
IL-15
Actin
Relative protein expression
0 μM 0.1 μM 0.5 μM 1 μM
B
Control
A23187
A23187+CsA
CnA
β-Actin
Relative protein expression
Control A23187 A23187+CsA
C
Control
A23187
A23187+CsA
NFATc1
Histone H3
Relative protein expression
Control A23187 A23187+CsA
D
Control
A23187
A23187+CsA
IL-15
β-Actin
Relative protein expression
Control A23187 A23187+CsA
E
Bits
-2000 bp
NFATc1
AATGGAAAA
Transcription
IL-15
-991
-999
F
NFATc1 and the key sequence of IL-15 promoter docking
Confidence Score: 0.8292
G
Probe name
Sequence
bio-NFATc1
Biotin-5'-TCAGTGTGAAATGGAAAAGTGGTTGGG-3'
3'-AGTCACACTTTACCTTTTCACCAACCC-5'-Biotin
cold-NFATc1
5'-TCAGTGTGAAATGGAAAAGTGGTTGGG-3'
3'-AGTCACACTTTACCTTTTCACCAACCC-5'
mu-NFATc1
5'-TCAGTGTGAAGCAGGGAGGTGGTTGGG-3'
3'-AGTCACACTTCGTCCCTCCACCAACCC-5'
H
bio-NFATc1 -982/-1009
NE
Competitor
Control
A23187
A23187+CsA
A23187
A23187
mut
1 2 3 4 5 6
I
pcDNA3.1
pcDNA3.1-NFATc1
1 μg/ml
0.5 μg/ml
1 μg/ml
NFATc1
β-Actin
J
pcDNA3.1-NFATc1 + pGL3-IL15
pcDNA3.1 + pGL3-IL15
pcDNA3.1-NFATc1 + pGL3
pcDNA3.1 + pGL3
Relative fluorescence intensity

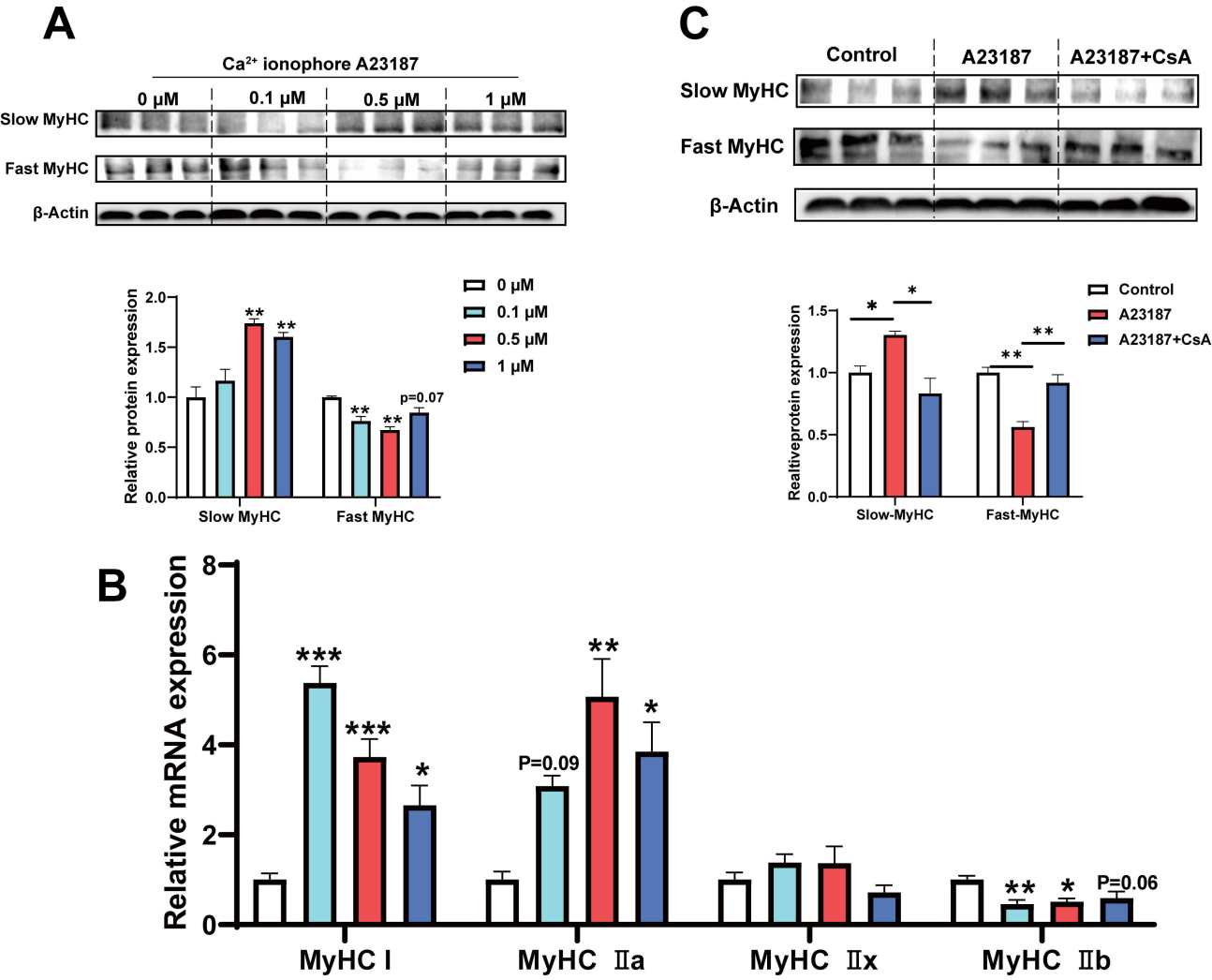
A
Ca2+ ionophore A23187
0 μM
0.1 μM
0.5 μM
1 μM
Slow MyHC
Fast MyHC
β-Actin
Relative protein expression
2.0
1.5
1.0
0.5
0.0
**
**
**
**
p=0.07
Slow MyHC
Fast MyHC
0 μM
0.1 μM
0.5 μM
1 μM
C
Control
A23187
A23187+CsA
Slow MyHC
Fast MyHC
β-Actin
Realtiveprotein expression
1.5
1.0
0.5
0.0
*
*
**
**
Slow-MyHC
Fast-MyHC
Control
A23187
A23187+CsA
B
Relative mRNA expression
8
6
4
2
0
***
***
*
P=0.09
**
*
**
*
P=0.06
MyHC Ⅰ
MyHC Ⅱa
MyHC Ⅱx
MyHC Ⅱb

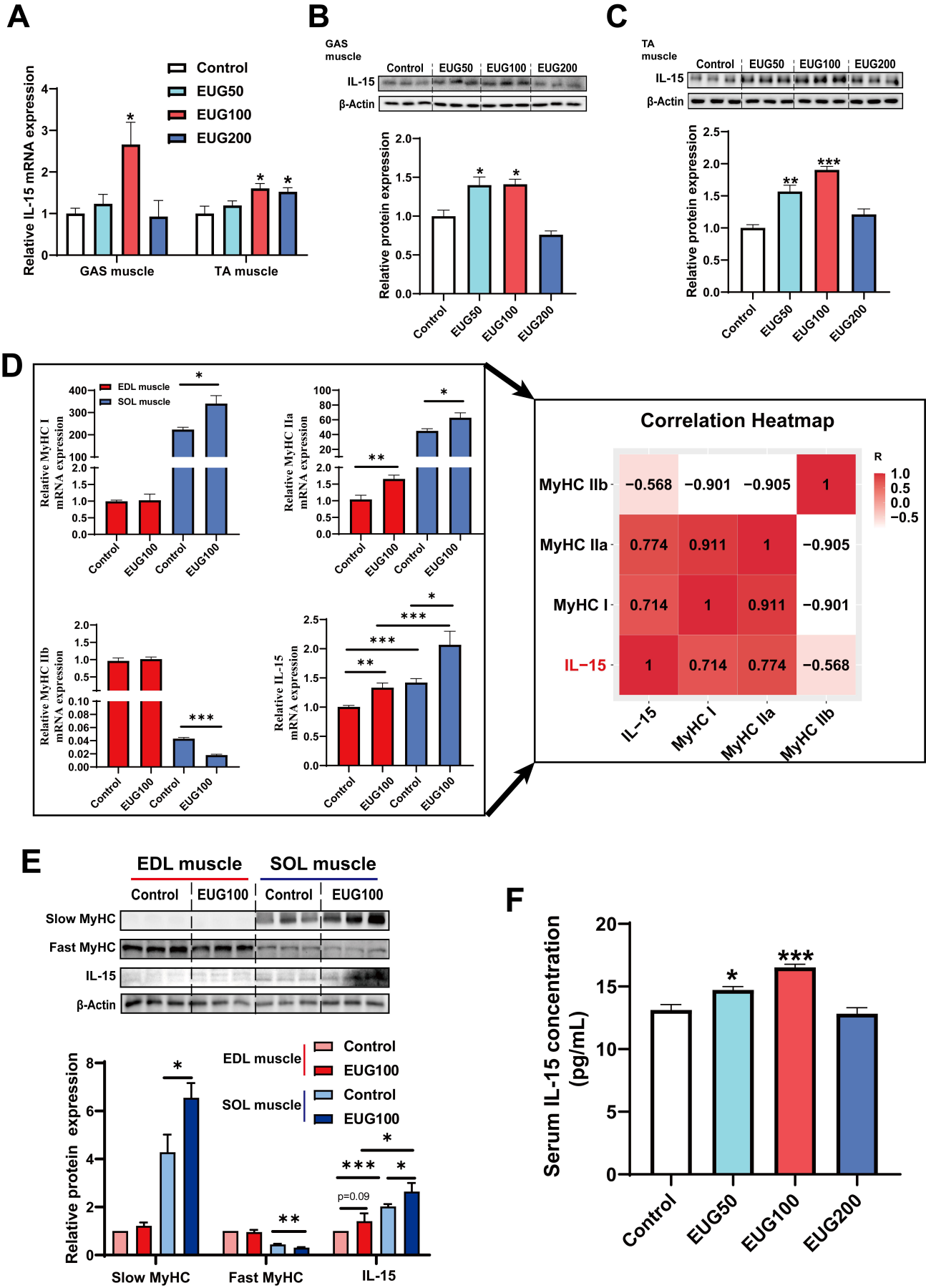
A
Control
EUG50
EUG100
EUG200
Relative IL-15 mRNA expression
GAS muscle
TA muscle
B
GAS muscle
Control
EUG50
EUG100
EUG200
IL-15
β-Actin
Relative protein expression
C
TA muscle
D
EDL muscle
SOL muscle
Relative MyHC I mRNA expression
Relative MyHC IIa mRNA expression
Relative MyHC IIb mRNA expression
Relative IL-15 mRNA expression
Correlation Heatmap
R
MyHC IIb
MyHC IIa
MyHC I
IL-15
E
EDL muscle
SOL muscle
Slow MyHC
Fast MyHC
IL-15
β-Actin
Relative protein expression
p=0.09
F
Serum IL-15 concentration (pg/mL)

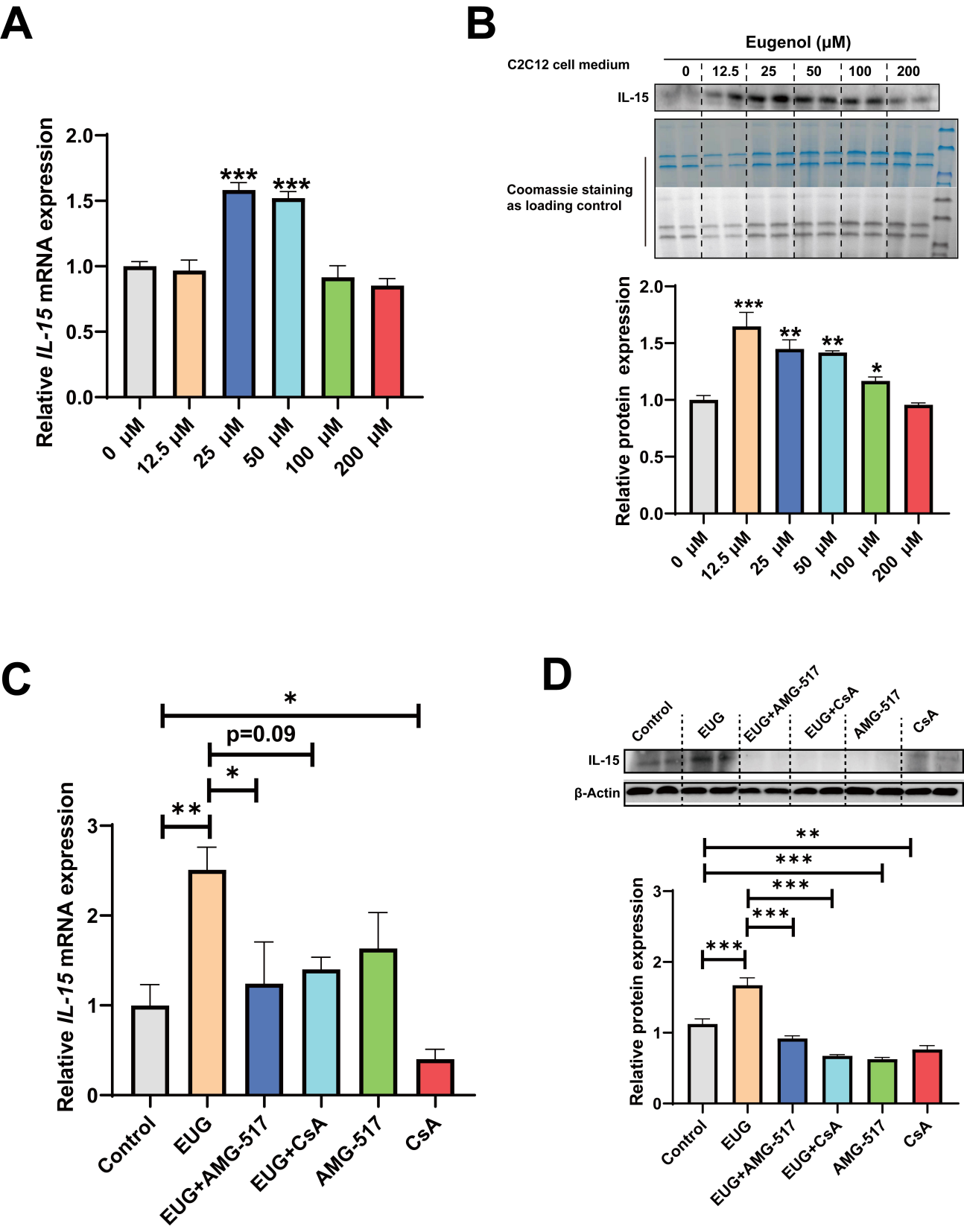
A
Relative IL-15 mRNA expression
2.0
1.5
1.0
0.5
0.0
***
***
0 μM
12.5 μM
25 μM
50 μM
100 μM
200 μM
B
Eugenol (μM)
C2C12 cell medium
0
12.5
25
50
100
200
IL-15
Coomassie staining as loading control
Relative protein expression
2.0
1.5
1.0
0.5
0.0
***
**
**
*
0 μM
12.5 μM
25 μM
50 μM
100 μM
200 μM
C
Relative IL-15 mRNA expression
3
2
1
0
*
p=0.09
*
**
Control
EUG
EUG+AMG-517
EUG+CsA
AMG-517
CsA
D
Control
EUG
EUG+AMG-517
EUG+CsA
AMG-517
CsA
IL-15
β-Actin
Relative protein expression
3
2
1
0
**
***
***
***
***
Control
EUG
EUG+AMG-517
EUG+CsA
AMG-517
CsA

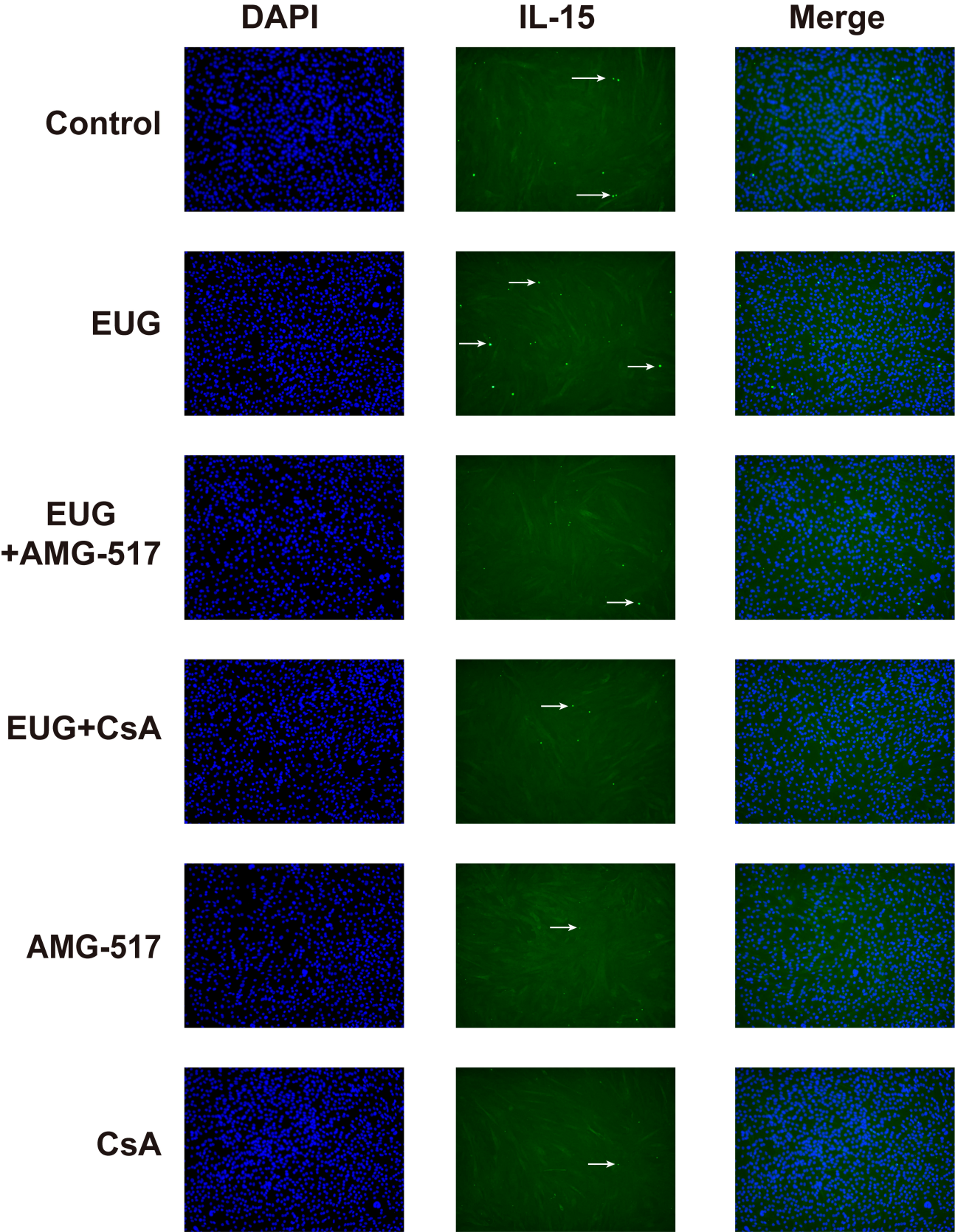
DAPI
IL-15
Merge
Control
EUG
EUG
+AMG-517
EUG+CsA
AMG-517
CsA